

**COLOR TRANSPARENCY EFFECTS IN
ELECTRON DEUTERON INTERACTIONS AT INTERMEDIATE Q^2**

L. L. Frankfurt

School of Physics and Astronomy, Tel Aviv University, 69978, Israel

Institute for Nuclear Physics, St. Petersburg, Russia

W. R. Greenberg

Department of Physics, University of Pennsylvania, Philadelphia, PA 19104

G. A. Miller

Department of Physics, University of Washington, Seattle, WA 98195

M. M. Sargsyan

School of Physics and Astronomy, Tel Aviv University, 69978, Israel,

Yerevan Physics Institute, 375036, Armenia

and

M. I. Strikman

Department of Physics, Pennsylvania State University, University Park, PA 16802

Institute for Nuclear Physics, St. Petersburg, Russia

Abstract

High momentum transfer electrodisintegration of polarized and unpolarized deuterium targets, $d(e, e'p)n$ is studied. We show that the importance of final state interactions FSI, occurring when a knocked out nucleon interacts with the other nucleon, depends strongly on the momentum \vec{p}_n of the spectator nucleon. In

particular, these FSI occur when the essential contributions to the scattering amplitude arise from internucleon distances $\sim 1.5 \text{ fm}$. But the absorption of the high momentum γ^* may produce a point like configuration, which evolves with time. In this case, the final state interactions probe the point like configuration at the early stage of its evolution. If the point like configuration is still small after propagating about 1.5 fm, the FSI are suppressed. The result is that significant color transparency effects, which can either enhance or suppress computed cross sections, are predicted to occur for $\sim 4\text{GeV}^2 \geq Q^2 \leq 10 (\text{GeV}/c)^2$. We suggest searching for color transparency phenomenon by examining ratios of experimentally measured quantities. Possible theoretical uncertainties of the calculations, including those due to the deuteron wave function and relativistic effects, are found to be small.

PACS: 25.30.-c; 25.30.Fj; 25.45.-z

1 Introduction

Color transparency (CT) and color coherent effects have been recently under intense experimental and theoretical investigation. The (p,pp) experiment of Carroll et al.[1] found indications of color transparency while the NE18 (e,e'p) experiment [2] found no such indications. The appearance of color transparency depends on formation of a point-like configuration (PLC) by hard scattering. The Q^2 of the NE18 experiment ($1 \leq Q^2 \leq 7\text{GeV}^2$) seem to be large enough to form a small color singlet object. The reason why significant color transparency is not observed is the rapid expansion of PLC to nearly normal size (a nearly normal absorption) at the relatively low momenta of the ejected protons[3, 4]. Thus models of color transparency which reproduce the (p,2p) data and include expansion effects predicted small CT effects for the NE-18 kinematics, consistent with their findings, see the discussion in Ref.[5].

Therefore a new strategy of using light nuclei and double scattering as a means to investigate whether small objects are produced at intermediate Q^2 was suggested in Ref.[6]. The idea was that using the lightest nuclei would allow the suppression of

expansion effects, while employing kinematical cuts to suppress the plane wave Born contributions and to enhance the contribution of double scattering interactions would increase the deviations from the Glauber model. That work concerned *He* nuclei target, in the present we use an improved formalism to investigate the use of a deuteron target.

The deuteron is the best understood nuclear system, with a wave function determined experimentally in a wide momentum range [7]. Therefore finding a method to use the deuteron to investigate color coherent -color transparency effects is both challenging and potentially rewarding. The average separation between the nucleons in the deuteron is large, so the deviations from the plane wave impulse approximation (PWIA) computed within the ordinary Glauber approximation are usually very small, much smaller than for a *He* target.

However a recent analysis of hard quasielastic $d(p, 2p)$ reactions within the framework of conventional Glauber approximation [8] has found substantial Glauber screening effects for transverse spectator momenta less than $300 \text{ MeV}/c$ and small longitudinal spectator momentum. In particular, the interference between the Born term and rescattering amplitude in which the knocked out nucleon interacts with the spectator nucleon, causes a reduction in the cross section. This is called a screening effect. Including the square of the rescattering amplitude, which we call the double scattering term, increases the computed cross section. Color transparency leads to a suppression of the rescattering amplitude, predicting specific upward and downward changes in the cross section, depending on the kinematics which control the relative sizes of the screening and double scattering terms. Thus observing such effects which occur for different values of the spectator momenta seems to be an effective method to search for color coherent effects using the deuteron.

Substantial screening has been observed also in the recent calculation [9] of the processes $d(e, e'p)$ within the nonrelativistic Glauber approximation. The present paper uses formulae of the Glauber approximation deduced from the Feynman diagrams. As a result the predicted angular dependence of the cross section at higher spectator momenta is noticeably different from that in Ref.[9]. In particular, the position in the spectator

angular distribution, corresponding to the maximal final state interaction depends on the momentum of the spectator nucleon. At $Q^2 \approx 1(\text{GeV}/c)^2$ our calculations agree well with calculations of Ref.[10, 11] in the kinematics where the double scattering term dominates. According to Ref.[10] in this kinematics the contribution of meson exchange currents and isobars in the intermediate is small. This is another example that the Glauber approximation is a good starting point in the hunt for the CT phenomenon.

We stress that exclusive processes of high momentum transfer electrodisintegration of the polarized and unpolarized deuteron - $d(e, e'p)n$ have an important advantage. One may choose special kinematical conditions for the spectator nucleon to control the essential internucleon distances ($\sim 1.5 \text{ fm}$) for final state interactions (FSI). Therefore it is possible to probe the PLC at the early stage of its evolution, where expansion effects are minimal. The chosen kinematics also allow the separate investigation of the different implications of CT for the screening and double scattering terms. Another limitation on the kinematics is the requirement of reliability of the nonrelativistic description of deuteron and smallness of competing nuclear effects which might diminish CT effects. The major price for fixing kinematics is the drop in the cross section, which should not cause a problem for high intensity accelerators.

The paper is organized as follows. In section 2 we calculate the cross section of the $d(e, e'p)n$ reaction within the framework of the conventional Glauber approximation[12]. Polarized and unpolarized targets are studied.

In section 3 color transparency effects in the $d(e, e'p)n$ reaction are calculated within the framework of quantum diffusion model[3] and three resonance model[13]. The three resonance model is solved in two ways: the Green function method of Ref.[6] and the modified Glauber approximation method, used previously to calculate nuclear vector meson production (see Refs.[14, 15, 16, 17]).

Section 4 contains the numerical results. We first use the Glauber approximation to investigate the kinematic requirements necessary to ensure the most favorable conditions for studying color coherent effects. This analysis allows us to introduce new experimental

observables which are free from theoretical normalizations and are more sensitive to the effects of final state interactions. Using the models, discussed in section 3, we calculate color transparency effects for the kinematic range accessible to the present generation of electron accelerators.

Section 5 considers theoretical uncertainties and the reliability of obtained results.

The main results of present paper are summarized in Section 6.

2 Glauber Approximation (GA)

We consider the $d(e, e'p)n$ reaction for kinematics in which the proton carries almost all of the momentum of the virtual photon and the neutron momentum p_n is in the range 200-400 MeV/c where deuteron wave functions have been determined experimentally.¹ The amplitude for $d(e, e'p)n$ processes can be expressed as the matrix element of the scattering operator - \hat{T} between the deuteron wave function and the wave function of the final state consisting of two outgoing nucleons:

$$\mathcal{M} = \int \int \langle \vec{p}_p, s_p; \vec{p}_n; s_n | \hat{T}(q) | d, \vec{s} \rangle d^3r_p d^3r_n. \quad (1)$$

Here $| d, \vec{s} \rangle$ is the position space deuteron wave function, $\vec{p}_p, \vec{r}_p, s_p$ and $\vec{p}_n, \vec{r}_n, s_n$ are the momenta, coordinate and spin of proton and neutron in the final state.

Within the conventional assumptions on factorization of hard - electromagnetic and soft - FSI amplitudes i.e. within the Glauber approximation the nuclear scattering operator has the coordinate space form:

$$\hat{T}(q, r_p, r_n) = T_S(p_p, p_n, r_p, r_n) \cdot T_H^{em}(Q^2) \cdot e^{i\vec{q} \cdot \vec{r}_p}, \quad (2)$$

where $T_H^{em}(Q^2)$ - is the one-body electromagnetic current operator, \vec{q} is the space component of the photon four-momentum which we choose in the z-direction. We note that

¹Obviously, kinematics in which the neutron is produced forward and proton sidewise is as good for our purposes. In fact, such a setup may have certain experimental advantages since in this case one detects neutron with the same momentum for different Q^2 . We thank B.Mecking for emphasizing this point.

factorization is violated when off-shell effects are taken into account. So we will focus on CT effects at small spectator nucleon momenta or in the rescattering region where only small momenta in the loop integral over internal nucleon momenta are important. We neglect the contributions of meson currents like that at Fig.1c since such contributions rapidly decrease with Q^2 for $x \sim 1$ (cf. discussion in [18] and sec. 5.5 below). $T_S(p_p, p_n)$ describes soft FSI of knocked-out proton with spectator neutron. We are studying situations in which the momentum of knocked - out proton is larger than $1 \text{ GeV}/c$. So T_S can be calculated within the Glauber approximation [12, 19, 20] ²:

$$T_S(p_p, p_n, r_p, r_n) = 1 - \Gamma^N(b_p - b_n) \cdot \Theta(z_n - z_p) \cdot e^{-i\Delta^0(z_p - z_n)}, \quad (3)$$

where $\vec{r} \equiv \vec{r}(z, \vec{b})$. Here the z direction is defined by the direction of the struck proton momentum \vec{p}_p . However within the considered kinematics, where proton carries almost all momentum of virtual photon, we choose for z the direction of \vec{q} . The profile function $\Gamma^N(b)$ is expressed via the nucleon -nucleon scattering amplitude (f^{NN}) as follows:

$$\Gamma^N(b) = \frac{1}{2i} \int \exp(i\vec{k}_t \cdot \vec{b}) \cdot f^{NN}(\vec{k}_t) \frac{d^2k_t}{(2\pi)^2}, \quad (4)$$

where the NN scattering amplitude normalized as $Imf^{NN}(k_t = 0) = \sigma_{tot}$. The additional factor $e^{-i\Delta^0(z_p - z_n)}$ in eq.(3), where

$$\Delta^0 = (E_n - m) \cdot \frac{m_d + q_0}{|\vec{q}|}, \quad (5)$$

is a kinematical factor. In eq.(5) E_n - is the spectator energy, m is the nucleon mass, m_d - is the mass of deuteron and q_0 is the transferred energy. The factor Δ^0 is obtained by evaluating Feynman diagrams (cf. section 5.4, eq.(58)) and accounts for the nucleon recoil usually neglected within the conventional non-relativistic Glauber approximation. This factor accounts for the fact that the variable $\frac{k_0 - k_z}{m}$ but not k_z (fig.1b) is conserved in two-body high energy collisions (cf. [21]).

²To simplify the discussion we neglect small corrections due to the charge exchange process $np \rightarrow pn$. Since the charge exchange amplitude is predominantly real and of spin flip character (which itself is small), it practically does not interfere with the main amplitude.

Inserting eqs.(3) and (4) into eq.(1), we obtain the amplitude for the $d(e, e'p)n$ reaction as:

$$\begin{aligned}
\mathcal{M} &= T_H^{em}(Q) \int \int d^3r_p d^3r_n e^{i\vec{q}\cdot\vec{r}_p} \langle \vec{r}_p, s_p; \vec{r}_n, s_n | d, \vec{s} \rangle \\
&\quad \times \left[1 - \Gamma(b_p - b_n) e^{-i\Delta^0(z_p - z_n)} \Theta(z_n - z_p) \right] e^{-i\vec{p}_p\cdot\vec{r}_p} e^{-i\vec{p}_n\cdot\vec{r}_n} \\
&= T_H^{em}(Q) \int \int d^3r_p d^3r_n e^{-i\vec{p}_i\cdot\vec{r}_p} e^{-i\vec{p}_n\cdot\vec{r}_n} \langle \vec{r}_p, s_p; \vec{r}_n, s_n | d, \vec{s} \rangle \\
&\quad - T_H^{em}(Q) \int \int_{z_p} d^3r_p d^3r_n e^{-i\vec{p}_i\cdot\vec{r}_p} e^{-i\vec{p}_n\cdot\vec{r}_n} \langle \vec{r}_p, s_p; \vec{r}_n, s_n | d, \vec{s} \rangle \\
&\quad \times \frac{1}{2i} \int e^{i\vec{k}_t\cdot(\vec{b}_p - \vec{b}_n)} \cdot f^{NN}(\vec{k}_t) \frac{d^2k_t}{(2\pi)^2} e^{-i\Delta^0(z_p - z_n)} \Theta(z_n - z_p), \tag{6}
\end{aligned}$$

where we define the momentum of initial proton in the deuteron state as $\vec{p}_i = \vec{p}_p - \vec{q}$.

To separate center-of-mass motion we introduce the center-of-mass (R_{cm}) and relative distance (r) coordinates:

$$\begin{aligned}
\vec{r}_p &= \vec{R}_{cm} + \frac{1}{2}\vec{r} \\
\vec{r}_n &= \vec{R}_{cm} - \frac{1}{2}\vec{r}. \tag{7}
\end{aligned}$$

Using Eq.(7) allows us to simplify Eq.(6) as:

$$\begin{aligned}
\mathcal{M} &= T_p^{em}(Q) \int d^3R_{cm} e^{i\vec{R}_{cm}\cdot(\vec{p}_d - \vec{p}_i - \vec{p}_n)} \left\{ \int d^3r \langle \vec{r}_p, s_p; \vec{r}_n, s_n | d, \vec{s} \rangle e^{-\frac{i}{2}\vec{p}_i\cdot\vec{r}} e^{\frac{i}{2}\vec{p}_n\cdot\vec{r}} \right. \\
&\quad \left. - \int d^3r \Theta(-z) \langle \vec{r}_p, s_p; \vec{r}_n, s_n | d, \vec{s} \rangle \cdot e^{-\frac{i}{2}\vec{p}_i\cdot\vec{r}} e^{\frac{i}{2}\vec{p}_n\cdot\vec{r}} \frac{1}{2i} \int e^{i\vec{k}_t\cdot\vec{b} - i\Delta^0 z} \cdot f^{NN}(\vec{k}_t) \frac{d^2k_t}{(2\pi)^2} \right\} \\
&= T_p^{em}(Q) \left\{ \int d^3r \langle \vec{r}_p, s_p; \vec{r}_n, s_n | d, \vec{s} \rangle e^{-i\vec{p}_i\cdot\vec{r}} \right. \\
&\quad \left. - \frac{1}{2i} \int \int d^3r \Theta(-z) \langle \vec{r}_p, s_p; \vec{r}_n, s_n | d, \vec{s} \rangle \cdot e^{-i(\vec{p}_i - \vec{k}_t)\cdot\vec{b} - i(p_{iz} + \Delta^0)\cdot z} f^{NN}(\vec{k}_t) \frac{d^2k_t}{(2\pi)^2} \right\}, \tag{8}
\end{aligned}$$

The integration over R_{cm} ensures the momentum conservation: $\vec{p}_n = -\vec{p}_i = \vec{q} - \vec{p}_p$. In the last part of eq.(8) we omit the factor $(2\pi)^3 \delta(\vec{p}_d - \vec{p}_p - \vec{p}_n)$, which will be included in the definition of cross section. (To simplify formulae we use the Laboratory frame, in which the momentum of the deuteron, \vec{p}_d is zero.)

The integration over the relative coordinate r leads to the result:

$$\mathcal{M} = (2\pi)^{\frac{3}{2}} \cdot T_p^{em}(Q) \left\{ \langle p_i, s_p, s_n | d, \vec{s} \rangle - \frac{1}{4i} \int \langle p'_i, s_p, s_n | d, \vec{s} \rangle f^{NN}(\vec{k}_t) \frac{d^2k_t}{(2\pi)^2} \right\}, \tag{9}$$

where $\vec{p}'_i \equiv (p_{iz} + \Delta^0, p_{it} - k_t)$ and $\langle p'_i, s_p, s_n | d, \vec{s} \rangle$ - is the deuteron wave function in momentum space representation. The additional factor $\frac{1}{2}$ in the second term is a consequence of $\Theta(-z)$ functions in eq.(8). (The accuracy of last replacement is discussed in sec.5.4).

Taking the square of the modulus of the amplitude and summing over the proton and neutron polarizations we obtain:

$$\begin{aligned} ||\mathcal{M}||^2 &\equiv \sum_{s_p, s_n, s'_p, s'_n} \mathcal{M}\mathcal{M}^\dagger \\ &= (2\pi)^3 \cdot |F_p^{e.m.}(Q^2)|^2 \cdot \left\{ \rho_d^{\vec{s}}(p_i, p_i) - \mathcal{R}e \frac{1}{2i} \int \frac{d^2 k_t}{(2\pi)^2} \rho_d^{\vec{s}}(p'_i, p_i) f^{NN^*}(k_t) \right. \\ &\quad \left. + \frac{1}{16} \int \int \frac{d^2 k_{t1} d^2 k_{t2}}{(2\pi)^4} \rho_d^{\vec{s}}(p_{i1}, p_{i2}) f^{NN}(k_{t1}) f^{NN^*}(k_{t2}) \right\}, \end{aligned} \quad (10)$$

where $\vec{p}_{i1} \equiv (p_{iz} + \Delta^0, p_{it} - k_{t1})$, $\vec{p}_{i2} \equiv (p_{iz} + \Delta^0, p_{it} - k_{t2})$.

In eq.(10) we introduced the deuteron density function:

$$\rho^{\vec{s}}(k_1, k_2) = \sum_{s_p, s'_p, s_n, s'_n} \langle k_2, s_p, s_n | d, \vec{s} \rangle \langle d, \vec{s} | k_1, s'_p, s'_n \rangle. \quad (11)$$

In this Glauber or distorted wave impulse approximation (DWIA) the $d(e, e'p)n$ cross section can be expressed as follows:

$$\frac{d\sigma}{dE_{e'} d\Omega_{e'} d^3 p_p} = \sigma_{ep} \cdot D_d(q, p_p, p_n) \cdot \delta(q_0 - M_d - E_p - E_n). \quad (12)$$

Here σ_{en} is the cross section of the electron scattering off a bound proton (up to the flux and proton recoil factor)³ and the decay function $D_d(q, p_p, p_n)$ represents the joint probability for the initial proton in the deuteron having Fermi momentum - p_i and for the final state having a proton and neutron with a momentum p_p and p_n (for more details see [22]).

³In principle, one should use the light-cone quantum mechanics of the deuteron [21] to calculate the cross section. However for the effects dominated by the contribution of small nucleon momenta in the deuteron of interest here, the difference between predictions of light-cone and nonrelativistic formalisms is small (see Sec.5.1).

If the deuteron is polarized, the cross section depends on $D_d^{\vec{s}}(q, p_p, p_n)$ with:

$$D_d^{\vec{s}}(q, p_p, p_n) = \rho_d^{\vec{s}}(p_i, p_i) - \mathcal{R}e \frac{1}{2i} \int \rho_d^{\vec{s}}(p_i, p'_i) \cdot f^{NN}(k_t) \cdot \frac{d^2 k_t}{(2\pi)^2} \\ + \frac{1}{16} \int \rho_d^{\vec{s}}(p_{i1}, p_{i2}) \cdot f^{NN}(k_{t1}) \cdot f^{NN*}(k_{t2}) \cdot \frac{d^2 k_{t1}}{(2\pi)^2} \frac{d^2 k_{t2}}{(2\pi)^2}. \quad (13)$$

The polarized density matrices of deuteron can be expressed via the s and d - wave components introducing the polarization vector \vec{a} according to Ref.[23]:

$$\rho_d^{\vec{a}}(k_1, k_2) = u(k_1)u(k_2) + \left[1 - \frac{3|k_2 \cdot a|^2}{k_2^2}\right] \frac{u(k_1)w(k_2)}{\sqrt{2}} + \left[1 - \frac{3|k_1 \cdot a|^2}{k_1^2}\right] \frac{u(k_2)w(k_1)}{\sqrt{2}} \\ + \left(\frac{9}{2} \frac{(k_1 \cdot a)(k_2 \cdot a)^*(k_1 \cdot k_2)}{k_1^2 k_2^2} - \frac{3}{2} \frac{|k_1 \cdot a|^2}{k_1^2} - \frac{3}{2} \frac{|k_2 \cdot a|^2}{k_2^2} + \frac{1}{2}\right) w(k_1)w(k_2), \quad (14)$$

where the components of \vec{a} are defined through the deuteron spin wave function as:

$$\psi^{10} = i \cdot a_z, \quad \psi^{11} = -\frac{i}{\sqrt{2}}(a_x + ia_y), \quad \psi^{1-1} = \frac{i}{\sqrt{2}}(a_x - ia_y), \quad (15)$$

where $\psi^{1\mu}$ is the projection of the deuteron's spin on the the μ direction. The unpolarized deuteron density matrix follows from Eq.(14) as:

$$\rho_d(k_1, k_2) = \frac{1}{3} \sum_a \rho_d^a(k_1, k_2) = u(k_1)u(k_2) + w(k_1)w(k_2) \cdot \left(\frac{3}{2} \frac{(\vec{k}_1 \cdot \vec{k}_2)^2}{k_1^2 k_2^2} - \frac{1}{2}\right). \quad (16)$$

3 Coherent Effects in $d(e, e'p)n$ Scattering

Theoretical analysis shows that in realistic models the absorption of a hard photon leads to the formation of a point like configuration, which undergoes a reduced interaction with other hadrons, because of its small size and its color neutrality [24]. To estimate the expected effects of color coherence we consider two different models which account for the formation of the PLC and their evolution to the normal hadronic state: quantum diffusion model of Ref.[3] and the three state model of Ref.[13].

3.1 Quantum Diffusion model (QDM)

The reduced interaction between the PLC and the spectator neutron can be accounted for by introducing the dependence of the scattering amplitude on the transverse size of PLC. However we consider energies that are far from asymptotic, so the expansion of PLC should be important. This feature is included by allowing the rescattering amplitude to depend on the distance from the photon absorption point. Including these effects leads to the modified deuteron decay function $D_d^{\bar{s}}(q, p_p, p_n)$:

$$\begin{aligned}
D_d^{\bar{s}}(q, p_p, p_n) &= \rho_d^s(u(p_i), w(p_i), u(p_i), w(p_i)) \\
&\quad - \mathcal{R}e \frac{1}{i} \int \rho_d^{\bar{s}}(u(p_i), w(p_i), \tilde{u}(p'_i)^*, \tilde{w}(p'_i)^*) f^{NN}(k_t) \frac{d^2 k_t}{(2\pi)^2} \\
&\quad + \frac{1}{4} \int \rho_d^s(\tilde{u}(p_{i1}), \tilde{w}(p_{i2}), \tilde{u}(p'_i), \tilde{w}(p'_i)) \frac{d^2 k_{t1}}{(2\pi)^2} f^{NN}(k_{t1}) f^{NN*}(k_{t2}) \frac{d^2 k_{t2}}{(2\pi)^2},
\end{aligned} \tag{17}$$

with the same form of $\rho_d^{\bar{s}}$ as in Eq.(14) but with modified radial wave functions:

$$\begin{aligned}
\tilde{u}(k) &= \frac{1}{(2\pi)^{\frac{3}{2}}} \int u(r) Y_0(\hat{r}) \cdot \frac{f^{PLC,N}(z, k_t, Q^2)}{f^{NN}(k_t)} \Theta(-z) e^{-i\vec{k}\cdot\vec{r}} d^3 r \\
\tilde{w}(k) &= \frac{1}{(2\pi)^{\frac{3}{2}}} \int w(r) Y_{20}(\hat{r}) \cdot \frac{f^{PLC,N}(z, k_t, Q^2)}{f^{NN}(k_t)} \Theta(-z) e^{-i\vec{k}\cdot\vec{r}} d^3 r.
\end{aligned} \tag{18}$$

Eq.(17) is derived in the same way as the Glauber formulae in the previous section. The only difference is to include the coordinate dependence of the rescattering amplitude. To calculate the deuteron decay function in the quantum diffusion model we model the amplitude of the $PLC - N$ scattering in a form[6] consistent with the optical theorem:

$$f^{PLC,N}(z, k_t, Q^2) = i\sigma_{tot}(z, Q^2) \cdot e^{\frac{b}{2}t} \cdot \frac{G_N(t \cdot \sigma_{tot}(z, Q^2)/\sigma_{tot})}{G_N(t)}, \tag{19}$$

where $b/2$ is the slope of elastic NN amplitude, $G_N(t)$ ($\approx (1 - t/0.71)^2$) is the Sachs form factor and $t = -k_t^2$. The last factor in eq.(19) accounts for the difference between elastic scattering of PLC and average configurations, using the observation that the t dependence of $d\sigma^{h+N \rightarrow h+N}/dt$ is roughly that of $\sim G_h^2(t) \cdot G_N^2(t)$ for not very large values of t and that $G_h^2(t) \approx \exp(R_h^2 t/3)$.

In Eq. (19) $\sigma_{tot}(l, Q^2)$ is the effective total cross section of the interaction of the PLC at the distance l from the interaction point. The quantum diffusion model [3] corresponds to:

$$\sigma_{tot}(l, Q^2) = \sigma_{tot} \left\{ \left(\frac{l}{l_h} + \frac{\langle r_t(Q^2)^2 \rangle}{\langle r_t^2 \rangle} \left(1 - \frac{l}{l_h}\right) \right) \Theta(l_h - l) + \Theta(l - l_h) \right\}, \quad (20)$$

where $l_h = 2p_f/\Delta M^2$, with $\Delta M^2 = 0.7 - 1.1 \text{ GeV}^2$. Here $\langle r_t(Q^2)^2 \rangle$ is the average transverse size squared of the configuration produced at the interaction point. In several realistic models considered in Ref.[24] it can be approximated as $\frac{\langle r_t(Q^2)^2 \rangle}{\langle r_t^2 \rangle} \sim \frac{1 \text{ GeV}^2}{Q^2}$ for $Q^2 \geq 1.5 \text{ GeV}^2$. Note that due to effects of expansion the results of calculations are rather insensitive to the value of this ratio whenever it is much less than unity.

3.2 Three-State Model

3.2.1 Summary of the model

To evaluate matrix element of operators T_S and T_H in eq.(1) we use the three-state model of Ref.[13]. The basic assumption of this model is that the hard scattering operator T_H acts on a nucleon to produce a non-interacting point-like configuration $|PLC\rangle$ which is a superposition of three baryonic states:

$$T_H|N\rangle = |PLC\rangle = \sum_{m=N, N^*, N^{**}} F_{m,N}(Q^2)|m\rangle, \quad (21)$$

where $F_{m,N}(Q^2)$ are elastic ($m = N$) and inelastic transition form factors in this model. It is important to notice that the transition form factors used here cannot be taken directly from data. This is because states N^* and N^{**} are *effective* states which, in fact, represent a number of actual physical states. In the following analysis we assume for certainty that all form factors have the same Q^2 -dependence. We neglect also possible spin effects in the form factors and in the operator T_H .

Color transparency is introduced in this model as the condition of lack of FSI at the point where PLC is produced:

$$T_S|PLC\rangle = 0. \quad (22)$$

It is this condition which distinguishes models with color transparency from models which include production of resonances and/or continuum in intermediate states[25]. Within the approximations discussed above T_S is equal to a matrix U which is the most general 3×3 (Hermitian) matrix that annihilates the PLC:

$$U = \sigma^{tot} \begin{pmatrix} 1 & \frac{-F_{N,N} + \epsilon F_{N^{**},N}}{F_{N^*,N}} & -\epsilon \\ \cdots & \mu & \frac{|F_{N,N}|^2 - \epsilon^* F_{N,N} F_{N^{**},N}^* - \mu |F_{N^*,N}|^2}{F_{N^*,N}^* F_{N^{**},N}} \\ \cdots & \cdots & \frac{\mu |F_{N^*,N}|^2 - |F_{N,N}|^2 + 2\text{Re}(\epsilon^* F_{N,N} F_{N^{**},N}^*)}{|F_{N^{**},N}|^2} \end{pmatrix}. \quad (23)$$

Taking account of the data on pp and pd diffractive scattering helps to restrict further the parameters of this matrix[13]. We use the matrix U from that work.

3.2.2 Green Function Method

In this section we use the Green function method developed in Ref.[6] to calculate CT effects in the double scattering reaction off 3He . Within this method, the matrix element for the process $d(e, e'p)n$ which includes final-state interactions, is equal to

$$\mathcal{M}^s(\vec{p}_p, s_p; \vec{p}_n, s_n) = \langle \vec{p}_p, s_p; \vec{p}_n, s_n | T_H + T_S G_0 T_H | d, \vec{s} \rangle, \quad (24)$$

where $\vec{p}_{p(n)}$ is the momentum of the recoil proton (neutron), $s_{p(n)}$ is the projection of the recoil proton (neutron) spin and s is the projection of the deuteron spin. T_H is the hard scattering operator - the electromagnetic current. G_0 is the free propagator, and T_S accounts for the soft final-state interaction. The matrix element \mathcal{M}^s is also a function of the four-momentum transfer Q^2 and the Bjorken variable x (or equivalently the virtual photon three-momentum \vec{q} and its energy q^0). However, this dependence will be omitted in the formulae to simplify notations. It is convenient to define

$$\mathcal{M}_0^s(\vec{p}_p, s_p; \vec{p}_n, s_n) = \langle \vec{p}_p, s_p; \vec{p}_n, s_n | T_H | d, \vec{s} \rangle, \quad (25)$$

$$\mathcal{M}_1^s(\vec{p}_p, s_p; \vec{p}_n, s_n) = \langle \vec{p}_p, s_p; \vec{p}_n, s_n | T_S G_0 T_H | d, \vec{s} \rangle. \quad (26)$$

The matrix element for the hard scattering operator is given by (cf eq.(21))

$$\langle m, \vec{r}_p, s_p; n, \vec{r}_n, s_n | T_H | d, \vec{s} \rangle = F_{m,N}(Q^2) e^{i\vec{q} \cdot \vec{r}_p} \langle \vec{r}_p, s_p; \vec{r}_n, s_n | d, \vec{s} \rangle. \quad (27)$$

Here m labels components in the PLC (N, N^*, N^{**}). The Green's function operator is diagonal in the hadronic mass eigenstate basis :

$$\langle m, \vec{r}_p, s_p; n, \vec{r}_n, s_n | G | m, \vec{r}_p', s_p; n, \vec{r}_n', s_n \rangle = -\frac{e^{ip_m |\vec{r}_p - \vec{r}_p'|}}{4\pi |\vec{r}_p - \vec{r}_p'|} \delta^{(3)}(\vec{r}_n - \vec{r}_n'). \quad (28)$$

Here p_m is the momentum of the m 'th component of the proton wavepacket. This is given by:

$$\begin{aligned} p_{mz} &= q - p'_{nz} \\ p'_{nz} &= \frac{Q^2(1 - \frac{1}{x}) + M_m^2 - M_N^2}{2q}. \end{aligned} \quad (29)$$

Here p'_{nz} is the momentum of the neutron spectator in the intermediate state (cf. discussion in sec. 5.4). The above expression is obtained using energy-momentum conservation in intermediate states, valid in the semiclassical approximation used here. The eq.(48) shows that when $|PLC\rangle$ state is modeled as a superposition with different masses, the longitudinal momentum of nucleons in the intermediate state differs from the longitudinal momentum of registered nucleons. This is another important difference of our three resonance model[13] from the model discussed in Ref.[25].

Here \hat{z} is the direction of the γ^* momentum, x is the Bjorken variable, and we take for simplicity $M_p = M_n = M_N$ and neglect the binding energy of the deuteron. The quantity M_m^2 is the squared mass of the m 'th component of the wavepacket state.

The matrix element of the final-state interaction operator T_S is parameterized according to eq.(23) with

$$\langle r_p, s_p; r_n, s_n | T_S | m, \vec{r}_p, s_p; m', \vec{r}_n, s_n \rangle = U_{m,p} \delta^{(3)}(\vec{r}_p - \vec{r}_n). \quad (30)$$

For the simplicity we neglect here the dependence of scattering amplitudes on momentum transfer (See however discussion in sec. 3.2.3).

We put all of the pieces together, insert complete sets of states, perform the integrals over the delta functions, and arrive at the following expression for the matrix elements:

$$\mathcal{M}_0^s(\vec{p}_p, s_p; \vec{p}_n, s_n) = F_{p,p}(Q^2) \int d^3r_p d^3r_n e^{-i\vec{p}_p \cdot \vec{r}_p} e^{-i\vec{p}_n \cdot \vec{r}_n} e^{i\vec{q} \cdot \vec{r}_p} \langle r'_p, s_p; \vec{4}_n s_n | d, \vec{s} \rangle, \quad (31)$$

$$\begin{aligned}
\mathcal{M}_1^s(\vec{p}_p, s_p; \vec{p}_n, s_n) &= i |\vec{p}_p| \sum_m U_{p,m} F_{m,p}(Q^2) \int d^3r e^{-i(\vec{k}_p + \vec{k}_n) \cdot \vec{r}_n} \\
&\quad \times e^{i\vec{q} \cdot \vec{r}_p} \frac{e^{ip_p m |\vec{r}_p - \vec{r}_n|}}{4\pi |\vec{r}_p - \vec{r}_n|} \langle \vec{r}_p, s_p; \vec{r}_n s_n | d, \vec{s} \rangle,
\end{aligned} \tag{32}$$

We introduce the relative and center-of-mass coordinates according to eq.(7), with this transformation, $d^3r_p d^3r_n = d^3R_{cm} d^3r$. The integral over d^3R_{cm} leads to momentum conservation: $\vec{q} = \vec{p}_p + \vec{p}_n$ in the Lab. frame of the deuteron. The remaining matrix elements are expressed purely in terms of the relative coordinate, \vec{r} .

The non-relativistic deuteron wavefunction [7] can be written in terms of the s - and d -state functions u and w as,

$$\langle \vec{r} | d, \vec{s} \rangle = \left[\frac{u(r)}{r} + \frac{w(r)}{\sqrt{8}r} S_{12}(\hat{r}) \right] |\vec{s} \rangle, \tag{33}$$

where the tensor operator

$$S_{12}(\hat{r}) = \frac{3\vec{\sigma}_p \cdot \hat{r} \vec{\sigma}_n \cdot \hat{r}}{r^2} - \vec{\sigma}_p \cdot \vec{\sigma}_n. \tag{34}$$

As a result of the angular integration in d^3r (in particular, the integration over azimuthal angle) $s_p + s_n = s$. It is, thus, convenient to define the quantities

$$\mathcal{M}_{0(1)}^s(\vec{p}_p, \vec{p}_n) \equiv \mathcal{M}_{0(1)}^s(\vec{p}_p, s_p; \vec{p}_n, s_n). \tag{35}$$

When $s = \pm 1$ then $s_p = s_n = \pm \frac{1}{2}$. When $s = 0$, then $\mathcal{M}_{0(1)}^s$ is symmetric combination of $s_p = -s_n = \frac{1}{2}$ and $s_p = -s_n = -\frac{1}{2}$. The amplitudes for the production of final-state proton are

$$\mathcal{M}_0^{s=\pm 1}(\vec{p}_p, \vec{p}_n) = 2\pi F_{pp}(Q^2) [\mathcal{U}_0 + \mathcal{W}_0], \tag{36}$$

$$\mathcal{M}_0^{s=0}(\vec{p}_p, \vec{p}_n) = 2\pi F_{pp}(Q^2) [\mathcal{U}_0 - 2\mathcal{W}_0], \tag{37}$$

$$\mathcal{M}_1^{s=\pm 1}(\vec{p}_p, \vec{p}_n) = 2\pi \sum_m U_{p,m} F_{m,p}(Q^2) [\mathcal{U}_m + \mathcal{W}_m], \tag{38}$$

$$\mathcal{M}_1^{s=0}(\vec{p}_p, \vec{p}_n) = 2\pi \sum_m U_{p,m} F_{m,p}(Q^2) [\mathcal{U}_m - 2\mathcal{W}_m], \tag{39}$$

where

$$\mathcal{U}_0 = 2 \int_0^\infty dr r u(r) \frac{\sin p_n r}{p_n r}, \quad (40)$$

$$\mathcal{W}_0 = \sqrt{2} \int_0^\infty dr r w(r) \left[\frac{\sin p_n r}{p_n r} + 3 \frac{\cos p_n r}{p_n^2 r^2} - 3 \frac{\sin p_n r}{p_n^3 r^3} \right], \quad (41)$$

$$\mathcal{U}_m = -\frac{2}{4\pi} \int_0^\infty dr e^{ip_{p_m} r} u(r) \frac{\sin qr}{qr}, \quad (42)$$

$$\mathcal{W}_m = -\frac{\sqrt{2}}{4\pi} \int_0^\infty dr e^{ip_{p_m} r} w(r) \left[\frac{\sin qr}{qr} + 3 \frac{\cos qr}{q^2 r^2} - 3 \frac{\sin qr}{q^3 r^3} \right], \quad (43)$$

and where $q = |\vec{q}|$ and $p_n = |\vec{p}_n|$. Note that $\mathcal{W}_0 = 0$ for $\vec{p}_n = 0$. At very high energies, $p_{p_m} \approx p_p$ is independent of m , so that \mathcal{U}_m and \mathcal{W}_m become independent of m . In this limit the matrix element \mathcal{M}_1^s is proportional to $\sum_m U_{p,m} F_{m,p} = 0$. This is the limit of full color transparency.

The formulae of the conventional Glauber approximation can be obtained from the above equations by retaining only the proton component in this sum.

3.2.3 Modified Glauber Approximation Approach

In this subsection we solve the three-state model using the method developed by Yennie [14], Kölbig and Margolis [15] and Bauer [16]. The major difference from the standard Glauber approximation is the modification of the profile function by substituting $f_{NN} \rightarrow f_{nm}$, where f_{nm} is the m -particle production amplitude and the phase factor due to the difference of the masses of particles n and m [16]. This differs from the previous subsection and provides an opportunity to include a non-zero range of the interaction (the slope b_m of the amplitude f_{nm}).

Thus we can use equations of section 2, and modify the profile function in eq.(3) to calculate the $d(e, e'p)n$ processes within the Three State Model:

$$\Gamma^N(b_p - b_n) \rightarrow \frac{1}{2} \sum_{m=N, N^*, N^{**}} \int U_{p,m} \frac{F_{m,p}}{F_{p,p}} e^{\frac{bm}{2}t} e^{i\vec{k}_t \cdot (\vec{r}_p - \vec{r}_n)} e^{-i\Delta_{m,p}(z_p - z_n)} \frac{d^2 k_t}{(2\pi)^2}, \quad (44)$$

where

$$\Delta_{m,p} \equiv |\vec{p}_m| - |\vec{p}_p| = \Delta^0 - \sqrt{M_N^2 + p_p^2} - M_m^2 - |\vec{p}_p| = \Delta^0 - \frac{M_m^2 - M_N^2}{2|\vec{q}|}. \quad (45)$$

In eq.(44) b_m is the slope factor of the transition amplitude. For the present analysis we will assume that slopes of all transition amplitudes are the same as for NN scattering. The factor $e^{i\Delta_{m,p}(z_p-z_n)}$ accounts for the phase shift due to the different masses of PLC components. The additional factor $\frac{F_{m,p}}{F_{p,p}}$ accounts for the different coefficients for $|PLC\rangle$ wave components. The main difference of eq.(44) from the formulae of the Generalized Glauber approximation[14, 15, 16, 17] is that eq.(44) should satisfy the sum rules eq.(22) in the point where PLC is produced ($z_p - z_n = 0$) and when $t \rightarrow 0$. Besides the effects of the m -dependence of t_{min} are effectively included in the sum rule eq.(22).

Using modified profile functions in the formulae for the transition operator in eq.(2) we obtain:

$$\begin{aligned} \mathcal{M} = & F_{p,p}(Q^2) \int d^3r \langle \vec{r}, s_p, s_n | d, \vec{s} \rangle \left\{ e^{-i\vec{p}_i \vec{r}} \right. \\ & \left. - \frac{1}{2i} \sum_m \int \frac{d^2k_t}{(2\pi)^2} U_{p,m} \frac{F_{m,p}}{F_{p,p}} e^{\frac{b_m}{2}t} \Theta(-z) \cdot e^{-i\Delta_{m,p}z} e^{-ip_i \cdot r} e^{ikt \cdot b} \right\}. \end{aligned} \quad (46)$$

The z -component for the momentum of knocked out proton in intermediate state is :

$$p_{iz}^m = p_{iz} + \Delta_{m,p}, \quad (47)$$

Finally we obtain the following expressions for the deuteron decay function:

$$\begin{aligned} D^d(q, p_p, p_n) = & \rho_d^{\vec{s}}(p_i, p_i) - \frac{1}{2} \sum_{m=P,N^*,N^{**}} \int \rho_d^{\vec{s}}(p_i, p_i^{m'}) \cdot U_{p,m} \frac{F_{m,p}}{F_{p,p}} \cdot e^{\frac{b_m}{2}t} \cdot \frac{d^2k_t}{(2\pi)^2} \\ & + \frac{1}{16} \sum_{m,m'} \int \rho_d^{\vec{s}}(p_{i1}^m, p_{i2}^{m'}) U_{p,m} \frac{F_{m,p}}{F_{p,p}} \cdot U_{p,m'}^\dagger \frac{F_{m',p}^\dagger}{F_{p,p}^\dagger} \cdot e^{\frac{b_m}{2}t_1} e^{\frac{b_{m'}}{2}t_2} \frac{d^2k_{t1}}{(2\pi)^2} \frac{d^2k_{t2}}{(2\pi)^2}. \end{aligned} \quad (48)$$

where $\vec{p}_i^{m'} \equiv \vec{p}_i^{m'}(p_{iz}^m, p_{it} - k_t)$, $\vec{p}_{i1}^m \equiv \vec{p}_{i1}^m(p_{iz}^m, p_{it} - k_{t1})$, $\vec{p}_{i2}^m \equiv \vec{p}_{i2}^m(p_{iz}^m, p_{it} - k_{t2})$, and density matrices $\rho_d^{\vec{s}}$ is same as defined in eq.(14).

4 Numerical Results

To estimate effects of final state interactions in the $d(e, e')n$ reaction we compare the predictions of different models (considered in sections 2 and 3) for the differential cross

section and the tensor polarization asymmetry with predictions of the plane wave Born impulse approximation.

The manifestations of color transparency depend strongly on the relative importance of the screening (interference term between Born (Fig.1a) and FSI amplitude (Fig.1b)) and double scattering terms (square of FSI amplitude). To separate different implications of CT it is necessary to distinguish kinematical conditions where one of these terms is dominant. Thus we analyze the deuteron decay function in eq.(13) defined in Glauber approximation, for the separate cases of unpolarized and polarized deuteron targets.

4.1 (e,e'p) scattering on unpolarized deuteron target

Consider first the unpolarized deuteron case. We define the transparency T as the ratio of the measured cross section (or calculated cross section with FSI) to the one calculated in the PWIA [1, 2, 3, 4, 26]:

$$T(Q^2, p_p, p_n) \equiv \frac{\sigma_{d(e,e'p)n}^{FSI}(Q^2, p_p, p_n)}{\sigma_{d(e,e'pn)}^{PWIA}(Q^2, p_p, p_n)}. \quad (49)$$

Within the Glauber approximation, the cross sections are controlled by the decay function in eq.(13) with the unpolarized density matrix of eq.(16). In Fig.2 the dependence of the transparency - $T(Q^2, p_p, p_n)$ on the spectator neutron angle θ_n is presented for different values of the spectator momenta - p_n at fixed $Q^2 = 6 (GeV/c)^2$. The figure demonstrates that the final state interaction is maximal for $\theta_n \approx 90^\circ$ at smaller spectator momenta ($\leq 200 MeV/c$) and the position of maximal FSI shifts to slightly lower spectator angles with increase of p_n . The shift is the consequence of kinematic factor Δ^0 of eq.(5) which accounts for the fact that for rescattering of energetic particles the $E_n - p_n^z$ component is conserved rather than p_n^z (see eq.(58) in section 5.4 below). As follows from eq.(58) the maximal FSI effect occurs at $x = \frac{Q^2}{2mq_0} = 1$, which provides the zero value of longitudinal momenta for intermediate spectator. Below we will refer to the exclusive kinematics corresponding to $x = 1$ as the perpendicular kinematics.

The fig.2 shows also that the final state interaction contributes differently to the re-

sulting cross section at different spectator momenta. At $p_n \leq 200 \text{ MeV}/c$ (Fig2.a,b) FSI is dominated by the screening effect (the second term in eq.(13)). At $p_n \geq 300 \text{ MeV}/c$ (Fig.2.c.d) the double scattering term (the third term in eq.(13)) plays the dominant role at the $x \approx 1$ and it tends to diminish the screening effects (dash-dotted curves in Fig.2). The sharp increase of the FSI with the increase of spectator transverse momenta is the consequence of the decrease of the values of actual impact parameters contributing to NN rescattering. Note that in calculations within the Glauber approximation the pn scattering amplitude have been estimated using the relation:

$$f^{pn} = \sigma_{tot}^{pn} \cdot (i + \alpha_n) e^{b_n/2t} \quad (50)$$

where $\alpha_n = \text{Ref}/\text{Im}f$ and parameters used are those of Refs.[26, 27, 28, 29].

The above analysis suggests that color transparency effects, which reduce the FSI (rescattering amplitude), will have different consequences for different intervals of spectator angles and momenta.

Results presented in Fig.3a indicate that transparency for the scattering off the deuteron in perpendicular kinematics ($x = 1$) should change quite dramatically with p_n from $T(p_n = 0) \approx 0.97$ down to $T(p_n = 0.2 \text{ GeV}/c) \approx 0.5$. The decrease of T shows that FSI, in this kinematical range, is mostly a screening effect (see Fig.2). Note that current NE-18 results[2] for T_d were obtained under assumption that T does not depend on p_t in the studied momentum range $p_t \leq 300 \text{ MeV}/c$. Therefore, to compare our results with these data it is necessary to perform a new analysis of the data with a more realistic nuclear model where $T(p_t)$ decreases with p_t .

However at $p_n \geq 300 \text{ MeV}/c$, $x = 1$ the transparency T starts to increase with spectator momentum (Fig.3b), since in this kinematics (see Fig.2) the double scattering term dominates.

As a consequence of different role of FSI in the considered two kinematics, CT effects will have nontrivial manifestations. CT will increase T as compared to GA predictions at $p_n \leq 200 \text{ MeV}/c$, $x = 1$ (see Fig.3a- curves "I,II,III") and will decrease T as compared to GA predictions at $p_n \geq 300 \text{ MeV}/c$, $x = 1$ (see Fig.3b- curves "IV,V").

The different pattern of CT effects for these two regions shows that the ratio of the cross sections:

$$R(Q^2, p_{n1}, p_{n2}) = \frac{\sigma(p_{n1} \approx 300, 400 \text{ MeV}/c)}{\sigma(p_{n2} \approx 200 \text{ MeV}/c)} \quad (51)$$

should be rather more sensitive to CT phenomenon. This quantity is more convenient to search for CT since it represents the ratio of directly measured experimental quantities, and does not require additional normalization to the corresponding PWIA calculation (as in eq(49)). In Fig.4 we present curves for the same kinematics as in Fig.3 where calculations accounting for CT effects are normalized to the corresponding Glauber approximation calculations. We calculate also the Q^2 dependence of the ratio- R (curves labelled by the boxes). One can see that CT can modify R by as much as 30% for Q^2 as low as $6 - 10 \text{ (GeV}/c)^2$. Note that this occurs in the kinematical region where competing nuclear effects in the deuteron are small and are under good theoretical control (see sec. 5).

In Fig.5 we compare the predictions of different CT approximations for transparency defined as in eq.(49). Comparison of calculations within the three resonance model shows that the Green function formalism (see sec.3.2.2) predicts smaller DWIA cross section (Fig.5 - solid lines labeled by boxes) than the modified GA approach (see sec.3.2.3). This difference is caused by the slope of the NN scattering amplitude in the modified GA approach. Including this effect allows the transverse internal nucleon momenta in the deuteron to be smaller in the modified GA approach. This is a qualitatively new feature. However, the effects of the finite range of interaction do not exceed 10% in the discussed kinematical range $p_n \leq 300 \text{ MeV}/c$. In the case of CT, for spectator momenta ($p_n \leq 200 \text{ MeV}/c$), neglecting the slope of the soft rescattering amplitude predicts approximately the same effects as modified GA (Fig.5a - dashed curves labeled by boxes). For larger spectator momenta ($p_n \geq 300 \text{ MeV}/c$) neglect of slope for rescattering amplitude enhances CT effect (Fig.5b - dashed curves labeled by boxes). This is because for higher spectator momenta rescattering occurs effectively at smaller distances than in the case of the modified GA. These considerations demonstrate that up to deuteron

internal nucleon momenta $\sim 200MeV/c$ one can neglect the finite sizes of the rescattered nucleons, while at higher momenta when internuclear distances become comparable with nucleon size one needs to account for the form factors of the interacting nucleons.

The energy dependence of final state interactions of the $d(e, e'np)$ reaction involving a spinless deuteron target has been recently discussed in Ref. [32]. That paper studies ratios of cross section integrated over p_t^n for various values of Bjorken x and uses the triple pomeron mechanism of diffraction, which is not applicable for the energies considered in this paper.

4.2 (e,e'p) scattering off the polarized deuteron

The possibility to employ a polarized deuteron target to investigate color coherent effects is quite tempting. Use of different polarization states enhances the role of the d -wave component of the deuteron wave function and so that smaller space-time intervals are probed. This results in tagging of the PLC at the early stage of its evolution to a normal hadron.

For numerical estimates we consider the tensor polarization T_{20} measurable in electrodisintegration of the polarized deuteron. We define T_{20} as:

$$T_{20} \equiv \frac{1}{3} (\sigma(1, 1) + \sigma(1, -1) - 2 \cdot \sigma(1, 0)) = \sigma_{ep} \cdot D_{20}^d(q, p_p, p_n) \cdot \delta(q_o - M_d - E_p - E_n), \quad (52)$$

where $\sigma(s, s_z) \equiv \frac{d\sigma^{\vec{s}, s_z}}{dE_{e'} d\Omega_{e'} d^3p_p}$, s and s_z are the spin and its z component of the deuteron. The decay function is defined according to Eq.(13) with the tensor polarization density function as:

$$\begin{aligned} \rho_{20}^d(k_1, k_2) &\equiv \frac{1}{3} \left(\rho_d^{\frac{-i}{\sqrt{2}}(a_x + ia_y)}(k_1, k_2) + \rho_d^{\frac{i}{\sqrt{2}}(a_x - ia_y)}(k_1, k_2) - 2 \cdot \rho_d^{i \cdot a_z}(k_1, k_2) \right) \\ &= \left[3 \frac{k_{2z}^2}{k_2^2} - 1 \right] \frac{u(k_1)w(k_2)}{\sqrt{2}} + \left[3 \frac{k_{1z}^2}{k_1^2} - 1 \right] \frac{u(k_2)w(k_1)}{\sqrt{2}} \\ &\quad + \left(\frac{3}{2} \left[\frac{(k_1 \cdot k_2) \cdot ((k_1 \cdot k_2) - 3k_{1z}k_{2z})}{k_1^2 k_2^2} + \frac{k_{1z}^2}{k_1^2} + \frac{k_{2z}^2}{k_2^2} \right] - 1 \right) w(k_1)w(k_2). \end{aligned} \quad (53)$$

Eqs.(14) and (15) are used in obtaining eq.(53).

For further calculations we define an asymmetry as the ratio of cross sections from a tensor polarized and unpolarized deuteron:

$$A_d(Q^2, p_p, p_n) \equiv T_{20} / \frac{d\sigma^{unp}}{dE_{e'} d\Omega_{e'} d^3p_p} = \frac{D_{20}^d(q, p_p, p_n)}{D_d^{unp}(q, p_p, p_n)}, \quad (54)$$

where the unpolarized decay function - $D_d^{unp}(q, p_p, p_n)$ is defined according to eq.(13) and (16).

Before considering manifestations of CT for T_{20} and A_d it is worthwhile to examine some properties of the tensor polarization density matrix eq.(53). Considering the scattering from unpolarized deuterons (section 4.1) demonstrates that FSI dominates for nearly perpendicular kinematics: $\vec{p}_s \perp \vec{q}$. Thus in Fig.6 we compare $\rho_{20}^d(k, k)$ at $k_z = 0$ with the corresponding unpolarized deuteron density function $\rho_d(k, k) = u(k)^2 + w(k)^2$ calculated with different (Paris and Bonn) NN potentials. Fig.6 illuminates several remarkable properties of the tensor polarization density functions. First, it practically coincides with unpolarized density function for $k \approx 300 \text{ MeV}/c$, where $u(k) \approx -\frac{w(k)}{\sqrt{2}}$. This property reflects the fact that the s - partial wave in the deuteron falls with k , and changes sign at $k \approx 400 \text{ MeV}/c$, while d -wave grows with k from negative minimum at $k \approx 100 \text{ MeV}/c$. Thus in some range of momenta, the influence of the d -state is comparable (or larger) than that of the s -state (for a more detailed discussion see [7]). Note that we follow here the convention of Refs.[30, 31] which define the deuteron wave function so that $w(k) < 0$ at small k . The opposite convention, corresponding to $w(k) > 0$ is adopted e.g. in Refs. [7, 22]). This equality of polarized and unpolarized density functions means that in this kinematical range the asymmetry calculated according to eq.(54) will be close to unity, for perpendicular kinematics provided there is no final state interaction (i.e. in the plane wave Born approximation). This prediction is practically independent of the NN potential used to compute the deuteron wave function (see Fig.6). Besides, we will see in sec.5 that other effects such as the EMC effect, off-shell and relativistic effects are small for our kinematics. So deviations of the asymmetry from unity originate predominantly from the influence of final state interactions.

The next important feature of the tensor polarization density function is that it decreases with decrease of internal momenta (Fig.6), and we find that average momenta in the integrals for the final state interactions in the perpendicular kinematics are 100 – 150 MeV/c . Therefore, within the framework of the conventional eikonal approximation large effects of FSI are expected, since rescattering occurs at rather small internucleon distances $\sim 1.5 fm$. This dominance of FSI by small internucleon distances indicates that the effect of PLC evolution to a normal size nucleon will be reduced. Therefore one should expect larger sensitivity to CT effects.

In Fig.7 we present a three-dimensional plot of the asymmetry A_d as a function of the spectator momenta and the polar angle, calculated within the PWIA (Fig.7a) and the Glauber approximation (Fig.7b). This figure clearly demonstrates the large influence of final state interactions within the framework of Glauber approximation for perpendicular kinematics with $p_n \approx 250 - 350 MeV/c$ and $\theta_n \approx 60 - 90^0$.

In Fig.8 the Q^2 dependence of A_d is calculated using the PWIA, Glauber approximation and CT models considered in text, for different values of spectator transverse momenta. The sensitivity to CT effects is noticeable.

In Fig.9 the Q^2 dependence for both the ratio $R(Q^2, p_{n1}, p_{n2})$ defined according to eq.(51) and asymmetry A_d defined according to eq.(54) calculated for different values of ΔM^2 , which determines the coherence length within the QDM prediction of color transparency. Here we restrict Q^2 to the range available at CEBAF in the near future ($Q^2 \sim 6 (Gev/c)^2$)[33]. One can see that already in the $E_e = 4 - 6 GeV$ CEBAF run, it is possible to obtain important constraints on the parameters of CT.

5 Theoretical uncertainties

In this section we consider several theoretical issues which might influence the reliability of our interpretation of the measured cross sections.

5.1 Relativistic motion of target nucleons

The fact that high energy processes develop along the light-cone can be taken into account within the framework of the light-cone mechanics[21, 22]. The light-cone calculation of processes involving a deuteron target is more straightforward than that using nonrelativistic quantum mechanics. The parameter which characterizes the importance of relativistic motion of nucleons in the deuteron is the difference between the deuteron internal momentum defined in the laboratory reference frame (p_n) and in the light-cone reference frame [21]:

$$k_n = \sqrt{\frac{m^2 + p_{nt}^2}{\alpha(2 - \alpha)}} - m^2, \quad (55)$$

where $\alpha = \frac{p_{n-}}{p_{d-}}$ is the light-cone fraction of deuteron momentum carried by spectator nucleon. In the perpendicular kinematics of present interest $\alpha \approx 1$ and it follows from eq.(55) that $k_n \approx p_{nt}$. Therefore the expected relativistic effects of nucleon motion in the deuteron are insignificant corrections ($\sim \mathcal{O}(1 - \alpha)^2$). Another potentially possible source of difference between nonrelativistic and light-cone descriptions is the nucleon spin rotation effect[34]. However it was demonstrated in Ref.[22] that in the case of perpendicular kinematics this difference is negligible once again. Note also, that relativistic effects are even less important for the FSI, since integrals in the FSI amplitude (see e.g. eq.(13)) are sensitive to rather smaller values of the deuteron internal momenta.

5.2 Uncertainties in knowledge of the deuteron wave function

Possible uncertainties in the calculation of the $d(e, e'p)n$ processes with polarized and unpolarized targets are small and under control for the kinematics considered here because nucleon momenta in the deuteron do not exceed $300 - 350 MeV/c$ and FSI terms are sensitive to smaller deuteron internal momenta. Another reason why our processes are less sensitive to the uncertainty of the deuteron wave function, is that we consider observables which are the ratios of experimental quantities in (nearly) similar kinematical conditions (see eqs.(51) and (54)).

5.3 Off shell effects

The target nucleons are bound in the deuteron; the square of their four momentum is not the square of their mass. The nucleons are off-shell. One needs to estimate the influence of this effect to calculate the cross section of eq.(12). We estimated the uncertainties due to these effects by considering the Born amplitudes of models which account differently for off-shell effects in σ_{ep} [35, 22]. The differences are very small, less than one percent or so.

One of the uncertainties originates from the deformation of the bound nucleon wave function. This deformation has been calculated in Ref.[36] for processes dominated by PLC. A similar effect arises within Skyrmion models of the two nucleon interaction[37]. The major effect is the suppression of the probability for PLC in bound nucleon due to the color screening phenomenon[22]. The influence of this effect can be estimated by rescaling the deuteron wave function for a nucleon with momentum k by the factor:

$$\delta(k) = \left(1 + \Theta(Q^2 - Q_0^2) \cdot \left(1 - \frac{Q_0^2}{Q^2} \right) \cdot \frac{\frac{k^2}{m} + 2\epsilon_d}{\Delta E} \right)^{-1}, \quad (56)$$

where ϵ_d is the deuteron binding energy and $\Delta E(\approx 0.6 \text{ GeV})$ is the parameter which characterize bound nucleon excitations in the deuteron. The Q^2 dependence accounts for the presumed dominance of PLC in bound nucleons for sufficiently large momentum transfer $Q^2 \geq Q_0^2 \approx 2(\text{GeV}/c)^2$ [26].

In Fig. 10 we present calculations of the ratio defined in eq.(51) (Fig.10a) and the asymmetry defined by eq.(54) (Fig.10b) which include the influence of the PLC suppression effect of Eq.(56). Figures demonstrate that considered uncertainties are on the level of 5% and 10% in the case of unpolarized and polarized measurements respectively.

5.4 Semiclassical approximation for FSI in the momentum space - Feynman diagram approach

When calculating FSI for the $d(e, e'p)n$ reaction we substituted $\Theta(-z)$ contribution in eq.(8) by $\frac{1}{2}$ (cf. Eq.(9)). This replacement allows to represent the FSI amplitude (Fig.1b) as the convolution integral of the deuteron wave function and the on-energy shell NN scattering amplitude in the momentum space. The aim of this subsection is to substantiate our approximations. We start by analyzing the Feynman diagram, Fig.1b, which describes the FSI. Our interest is in the kinematics where the momentum of the nucleon-spectator - p_n is small: $\frac{p_n^2}{m_n^2} \ll 1$. In this case it is reasonable to consider the nonrelativistic motion of the nucleon in the deuteron: $\frac{p_n'^2}{m_n^2} \ll 1$, where p_n' is the momentum of spectator in the intermediate state ($\vec{p}'_n = \vec{p}_n - \vec{k}$, k is transferred momentum in the amplitude of FSI - see Fig1.b). So it is legitimate to evaluate the loop integral by taking a residue over the energy of the spectator nucleon in the intermediate state - p'_{n0} . (For nonrelativistic motion of the nucleon this is the only pole in the lower part of the complex plane in the variable p'_{n0} .) Neglecting systematically all the terms $\sim \frac{p_n'^2}{m_n^2}$ as compared to 1 we obtain:

$$\frac{\mathcal{M}^{FSI}}{\langle p' | J_\mu^{em} | p \rangle} = -\frac{(2\pi)^{\frac{3}{2}}}{2} \int \psi(p'_n) \frac{f^{NN}(p'_n - p_n, s)}{p'_{nz} - p_{nz}^0 + i\epsilon} \frac{d^3 p'_n}{(2\pi)^3} \quad (57)$$

Here the momentum \vec{q} is chosen to be in the z axis direction, $s = (p_d^\mu + q^\mu)^2$ and:

$$p_{nz}^0 \equiv (x-1)m \frac{q_0}{\sqrt{Q^2 + q_0^2}} = p_{nz} - \Delta^0 = p_{nz} - (E_n - m) \frac{M_d + q_0}{\sqrt{Q^2 + q_0^2}} \quad (58)$$

where p_{nz} is the z -component of measured spectator momentum. The last term of eq.(58) accounts for real kinematics of the considered process. The amplitude f^{NN} in the eq.(57) is normalized according to $Im f^{NN}(s, t=0) = \sigma_{tot}$ and the deuteron wave function normalized as $\int \psi^2(p_n) d^3 p_n = 1$.

Eq.(58) reflects an important property of two-body high energy processes in which the variable $k_- = k_0 - k_z$ (fig.1b) but not k_z is small. This dynamics is easily accounted for in light-cone mechanics of deuteron [21].

It is easy to demonstrate that eq.(57) is equivalent to the usual Glauber approximation if off-energy shell effects are neglected in f^{NN} . Really, if we use the Fourier transform of the deuteron wave function as:

$$\psi(p'_n) = \frac{1}{(2\pi)^{\frac{3}{2}}} \int \psi(r) e^{-i\vec{p}'_n \vec{r}} d^3r \quad (59)$$

the integral in eq.(57) over p'_{nz} differs from 0 for $z < 0$ only. This is the factor $\Theta(-z)$ in the coordinate space representation.

We shall neglect in the following analysis the dependence of f^{NN} on p'_{nz}, p_{nz} , since they are small for two body processes at high energies and will ignore off shell effects for small momenta of spectators. Then the integral over p'_{nz} can be evaluated by deforming the contour integral over p'_{nz} into the lower part of the complex plane. To calculate this integral we need to know analytic properties of the wave function of deuteron. For this we use the conventional parametrization of deuteron wave function calculated with Paris[30] and Bonn[31] NN potentials:

$$\psi(p) = \sum_j \frac{C_j}{p^2 + m_j^2} \quad (60)$$

where $\sum_j C_j = 0$ and s and d -waves differ by coefficients C_i . Substituting $\psi(p'_n)$ in eq.(57) from eq.(60) we obtain:

$$\begin{aligned} \frac{\mathcal{M}^{FSI}}{\langle p | J^e m_\mu | p \rangle} &= -\frac{(2\pi)^{\frac{3}{2}}}{2} \sum_j \int \frac{d^2 p'_{n\perp}}{(2\pi)^2} \int \frac{d^2 p'_{nz}}{(2\pi)} \times \\ &\quad \frac{C_j}{(p'_{nz} + i\sqrt{p'^2_{n\perp} + m_j^2})(p'_{nz} - i\sqrt{p'^2_{n\perp} + m_j^2})} \frac{f^{NN}}{p'_{nz} - p_{nz} + i\epsilon} \\ &= \frac{i}{2} \sum_j \int \frac{d^2 p'_{n\perp}}{(2\pi)^2} f^{NN} \left[\frac{C_j}{\tilde{p}_n^2 + m_j^2} - \frac{iC_j(p_{nz}^0 - i\sqrt{p'^2_{n\perp} + m_j^2})}{2\sqrt{p'^2_{n\perp} + m_j^2}(\tilde{p}_n^2 + m_j^2)} \right] \quad (61) \end{aligned}$$

where $\tilde{p}_n \equiv (p_{nz}^0, p'_{n\perp})$. Separating the real and imaginary parts inside of [...] and using eq.(60) one obtains a factor $\frac{1}{2}$ which we used in eq.(8) and additional term neglected in the above calculations:

$$\begin{aligned} \frac{\mathcal{M}^{FSI}}{\langle p | J^e m_\mu | p \rangle} &= \frac{i}{2} \int \frac{d^2 p'_{n\perp}}{(2\pi)^2} f^{NN} \left[\frac{\psi(\tilde{p}_n)}{2} - \frac{ip_{nz}^0}{2} \sum_j \frac{C_j}{\sqrt{p'^2_{n\perp} + m_j^2}(\tilde{p}_n^2 + m_j^2)} \right] \\ &= \frac{i}{4} \int \psi(\tilde{p}_n) f^{NN} \frac{d^2 p'_{n\perp}}{(2\pi)^2} \times \{1 - i\beta\}, \quad (62) \end{aligned}$$

where

$$\beta = \frac{p_{nz}^0 \int \frac{d^2 p'_{n\perp}}{(2\pi)^2} f^{NN} \sum \frac{C_j}{\sqrt{p'^2_{n\perp} + m_j^2} \cdot (\tilde{p}_n^2 + m_j^2)}}{\int \psi(\tilde{p}_n) f^{NN} \frac{d^2 p'_{n\perp}}{(2\pi)^2}}. \quad (63)$$

The size of β is a measure of the accuracy of replacing the $\Theta(-z)$ function by the factor $\frac{1}{2}$. Eqs.(62), (58) and (63) show that within the Glauber approximation the contribution from the factor β decreases with spectator longitudinal momentum p_{nz} and is practically negligible for perpendicular kinematics. However in the case of the modified Glauber approximation for the three resonance model (sec.3.2.3) the longitudinal momentum of intermediate state does not coincide with the longitudinal momentum of external detected particle. Due to this difference, the value of β in the three resonance model is determined at $p'_{nz} = p_{nz}^0 - \Delta_{m,p}$, where $\Delta_{m,p}$ is defined according to eq.(45). Therefore the contribution of β will be larger than within the conventional Glauber approximation. Note that contribution of $\Delta_{m,p}$ in soft FSI are effectively included into the sum rule eq.(22).

It follows from eq.(62) that the contribution of β factor to the interference of Born and FSI amplitude is further suppressed because the real part of f^{NN} amplitude is small (~ 0.2 of the imaginary part) and because the Born term corresponding fig1.a is real. The contribution of β factor to the double scattering term is $\sim \beta^2$ (cf. eq.(62)).

In Fig.11 we demonstrate the Q^2 dependence of the ratio defined by eq.(51) (Fig.11a) and the asymmetry defined by eq.(54) (Fig.11b) within the conventional Glauber approximation and the modified Glauber approximation for the three resonance model. It follows from this calculation that including β within the three resonance model of modified GA brings the predictions of this model and QDM approximation (where we included the $\Theta(-z)$ factor explicitly in coordinate space) closer together.

5.5 Meson exchange currents (MEC) and Δ -isobar contributions

Estimates of contributions from meson exchange currents corresponding to diagrams similar to Fig.1c are rather controversial at large Q^2 since these terms are very sensitive to the assumed t -dependence of the meson-nucleon vertex form factors. These form factors are not obtained from theory; instead they are used as fitting parameters[38]. On the other hand the restriction to $x = \frac{Q^2}{2mq_0} \approx 1$ and $Q^2 \geq 1 (GeV/c)^2$ strongly suppresses the sea quark content in nucleons. Including mesonic components is one way to treat the anti-quark content, so that a suppression of the sea can be considered as a hint of the suppression of MEC at large Q^2 and $x \geq 1$. This argument relies on the Bloom-Gilman duality [39] between the structure function of a nucleon at $x \rightarrow 1$ and contribution of resonances and on the fact that this hypothesis describes reasonably near threshold data for deep inelastic eN scattering. Besides, the diagram corresponding to Fig.1c contains an extra $\frac{1}{Q^2}$ factor as compared to the Born (Fig.1a) and the FSI (Fig.1b) diagrams.

The Δ -isobar contribution is expected to be small also in the kinematical range suitable for studying CT effects, since the $\gamma^*N \rightarrow \Delta$ transition form factor decreases more rapidly with Q^2 than the N^* transition form factors[40]. Another reason for the suppression of the contribution of Δ 's is that the $\Delta N \rightarrow NN$ amplitude is predominantly real and decreases rapidly with energy (since it is dominated by pion exchange) whereas the FSI effects we study are determined by imaginary part of the soft rescattering amplitude.

In fig.12 we compare predictions of the Glauber approximations of this paper with results of calculations of the model of Ref.[10].⁴ Calculations has been performed in the kinematics $Q^2 = 1 (GeV/c)^2$, $q_0 \sim 400 - 500 MeV/c$ and spectator momentum $p_n = 400 MeV/c$. Within model of Ref.[10] the contribution of meson currents and isobars in the kinematics where NN rescattering dominates is small ($\sim 6\%$ for MEC and $\sim 4\%$ for isobar contribution). Comparison of our approach and that of Ref.[10]

⁴We are thankful to W. Leidemann for making available his calculations within the approach of Ref.[10] for the kinematics discussed in this paper.

hints that Glauber approximation is applicable for Q^2 as small as 1 $(GeV/c)^2$. Note that calculation according to Ref.[10] can be considered as the upper limit for the contribution of meson currents. Theoretical analyses of current data (cf. Ref.[41]) and calculations of Ref.[42] indicate that the contributions of meson exchange currents have been strongly overestimated previously.

5.6 Charge exchange contribution and spin dependence of the elementary amplitude

In this analysis we have neglected contributions of terms in which the large longitudinal momentum is first transferred to the neutron which then converts to a proton via a charge exchange process. Since the charge exchange reaction $np \rightarrow pn$ is dominated by the pion exchange its amplitude is predominantly real. Therefore it mostly contributes to the double interaction term, not to the screening term. We can estimate its relative contribution as

$$\frac{\sigma_{chargeexchange}}{\sigma_{double}} \approx \frac{\sigma_{en,elastic} \frac{d\sigma^{np \rightarrow pn}}{dt}}{\sigma_{ep,elastic} \frac{d\sigma^{pn \rightarrow pn}}{dt}} \Big|_{t \sim 0.05(GeV/c)^2} \quad (64)$$

Using the data from Ref. [43], we estimate that this correction is of the order of 9% for $Q^2 \sim 2GeV^2$ and it decreases rapidly with Q^2 , approximately as Q^{-4} . For the case of leading neutron production, the relative contribution of the charge exchange is larger by a factor $\sigma_{ep}^2/\sigma_{en}^2 \leq 5$. Note that we expect transparency effects to cut down the charge exchange just as they reduce elastic scattering. This is the chiral transparency effect discussed in Ref. [24]; so this charge exchange effect does not affect our conclusions concerning the sensitivity of the $d(e, e'p)n$ reaction to color coherent effects.

Note also that we neglected another effect of dependence of the elastic pn amplitude on the parallel or anti-parallel nature of the helicities of the colliding nucleons. If we consider, for certainty, magnetic transitions, the rescattered nucleons will predominantly be in the antiparallel (parallel) state for $\lambda_d = 1(0)$. Using the current data on the $\sigma_L^{tot}(pn)$ difference [44], we estimate that this effect leads to a correction to the rescattering

amplitude which is $\leq 3\%$ for $Q^2 \sim 2(\text{GeV}/c)^2$ and $\leq 1\%$ for $Q^2 \sim 4(\text{GeV}/c)^2$. This effect is somewhat more important for A_d calculations. We will consider the effects discussed here in more detail elsewhere.

5.7 Factorization approximation

In the DWIA form of cross section (eq.(12)) we assume that the electron-nucleon cross section is not changed by the distortion of kinematics due to final state interaction. This commonly used assumption for the distorted wave impulse approximation allows us to factorize the cross section in the form of eq.(12). However computing the unfactorized form of cross section for the deuteron is quite straightforward and the authors will discuss it elsewhere. For small nucleon momenta within deuteron this effect is small anyway.

6 Summary

We have demonstrated that selecting perpendicular kinematics for the spectator: $p_n \sim 200 - 400 \text{ MeV}/c$, $x \sim 1$ significantly increases the effect of struck nucleon rescattering off the spectator nucleon. Thus varying p_n allows the selection of smaller than average internucleon distances in the FSI. If p_n is small the final state interactions cause a screening effect, and the effect of including the color transparency is to increase the computed cross section over the value obtained using the Glauber approximation. But for larger values of p_n , the conventional final state interactions enhance the cross section. In this case, the influence of color transparency is to suppress the computed cross sections. Based on these observations, we suggest measuring the ratio of $d(e, e'p)n$ cross sections, where in one case FSI is dominated by screening effect and in the second case by the double scattering. This ratio is more sensitive to the effects of color transparency. Our calculations of this ratio, using several CT models, predict 20 – 40% CT effects for $Q^2 \sim 4 - 10 (\text{GeV}/c)^2$.

High sensitivity of the $d(e, e'p)n$ cross section to the final state interaction of suffi-

ciently energetic struck nucleon is one of the preconditions for looking for color transparency phenomena. This condition is valid in the case of high energy electrodisintegration of a polarized deuteron with production of a spectator under the perpendicular kinematics discussed above. We suggest measuring the tensor asymmetry in $\vec{d}(e, e'p)n$ reaction, where conventional Glauber approximation predicts a huge influence of FSI. The dominance of deuteron d -state wave in the polarized density matrix restricts the essential internucleon distances to $\sim 1.5 \text{ fm}$, and suppresses the PLC evolution to a normal size nucleon. The CT models we consider give predictions of 50 – 100% effects at $Q^2 \sim 4 - 10 \text{ (GeV/c)}^2$.

To estimate the possibility for the unambiguous investigation of CT effects with deuteron target we considered a number of theoretical issues which might affect the reliability of the theoretical calculation of the $d(e, e'p)n$ reaction. The analysis shows that under our perpendicular kinematic conditions one can confine the theoretical uncertainties to the level of $\sim 5\%$ and $\sim 10\%$ for unpolarized and polarized measurements respectively.

Comparison with models explicitly accounting for meson currents and isobars shows that in the perpendicular kinematics preferable for searching for CT effects the deuteron can be considered as a clean detector with a low rate of noise.

7 Acknowledgments

This work was supported in part by the U.S.A. - Israel Binational Science Foundation Grant No. 9200126 and by the U.S. Department of Energy under Contract Nos. DE-FG02-93ER40771 and DE-FG06-88ER40427.

References

- [1] A. S. Carroll et al. *Phys. Rev. Lett.*, **61** 1698 (1988).

- [2] N. C. R. Makins et al. *Phys. Rev. Lett.* **72**, 1986 (1994)
- [3] G. R. Farrar, L. L. Frankfurt, M. I. Strikman and H. Liu, *Phys Rev Lett.* **61** 686 (1988).
- [4] B. K. Jennings and G. A. Miller, *Phys Lett.* **B236** 209 (1990); *Phys. Rev.* **D44**, 692 (1991); *Phys. Rev. Lett.* **70** 3619 (1992); *Phys. Lett.* **B274** 442 (1992).
- [5] L. L. Frankfurt, G. A. Miller and M. I. Strikman, *The Geometrical Color Optics of Coherent High Energy Processes, Ann. ReV. of Nucl. and Particle Phys.* 44,501, 1994.
- [6] K. Sh. Egiyan, L. L. Frankfurt, W. R. Greenberg, G. A. Miller, M. M. Sargsyan, and M. I. Strikman, *Nucl. Phys.* **A580**, 365 (1994).
- [7] G. E. Brown and A. D. Jackson, *The Nucleon-Nucleon Interaction, North-Holland Publish.Comp.*, 1976.
- [8] L. L. Frankfurt, E. Piasetsky, M. M. Sargsyan and M. I. Strikman, NUCL/TH-9405003 May 1994, *Phys. Rev. C*, in press.
- [9] A. Bianconi, S. Jeschonnek, N. N. Nikolaev and B. G. Zakharov, NUCL/TH-9409014, September 1994.
- [10] H. Arenhoevel, W. Leidemann, E. L. Tomusiak, *Phys. Rev.* **C46** 455 (1992).
- [11] W. Leidemann, *private communications*.
- [12] R. G. Glauber, *Lectures in Theoretical Physics, v.1*, ed. W. Brittain and L. G. Dunham, Interscience Publ., N.Y. 1959.
- [13] L. L. Frankfurt, W. R. Greenberg, G. A. Miller and M. I. Strikman, *Phys. Rev.* **C46** 2547 (1992).

- [14] D. R. Yennie, in *Hadronic interaction of Electrons and Photons* ed. J. Cummings and D. Osborn, 321 (1971).
- [15] K. S. Kölbig and B. Margolis, *Nucl. Phys.*, **B6**, 85 (1968).
- [16] T. Bauer, *Phys. Rev. Lett.*, **25**, 485, (1970). 85 (1968).
- [17] T. H. Bauer, R. D. Spital, D. R. Yennie and F. M. Pipkin, *Rev. of Mod. Phys.*, **v.50**, 261, (1978).
- [18] L. L. Frankfurt, L. L. Grach, L. A. Kondratyuk and M. I. Strikman, *Phys. Rev. Lett.* **62** 387 (1989).
- [19] V. Franco and R. G. Glauber *Phys. Rev.* **142** 1195 (1966).
- [20] L. Bertocchi and A. Capella *Il Nuovo Cimento* A51 369 (1967).
- [21] L L. Frankfurt and M. I. Strikman, *Phys.Rep.* **76** 214 (1981).
- [22] L L. Frankfurt and M. I. Strikman, *Phys.Rep.* **160** 235 (1988).
- [23] A B. Akhiezer and V. M. Berestecky, *Quantum Electrodynamics* Publish. - (1969).
- [24] L. L. Frankfurt, G. A. Miller and M. I. Strikman, *Comments on Nucl.Phys.* **21** 2547 (1992); L.Frankfurt, G.A.Miller, and M.Strikman, *Nucl.Phys.* **A555** 752 (1993).
- [25] B. Z. Kopeliovich *High Q^2 Probe of Nuclear Spectral Function and Color Transparency*, HEPPH-9311275, (1993), B. K. Jennings and B. Z. Kopeliovich *Phys.Rev.Lett.* **70** 3384 (1993).
- [26] L. L. Frankfurt, M. I. Strikman and M. Zhalov, *Phys. Rev.* **C50** (1994).
- [27] W. R. Greenberg and G. A. Miller, *Color Transparency and Dirac-Based Spin Effects in $(e, e'p)$ Reactions*, *Phys. Rev.* **C49**,2747 (1994)
- [28] B. H. Silverman *et al.* *Nucl. Phys.* **A499** 763 (1989).

- [29] *Review of Particle Properties*, *Phys. Rev* **D50** 1173 (1994).
- [30] M. Lacombe, B. Loiseau, R. Vinh Mau, J. Cote, P. Pires, R. de Tournell, *Phys. Lett.* **101B** 139 (1981).
- [31] R. Machleidt, K. Holinde and C. Elster, *Phys. Rep.* **149** 1 (1987).
- [32] V. V. Anisovich, L. G. Dakhno and M. M. Giannini, *Phys. Rev.*, **C49** 3275 (1994).
- [33] *Workshop on CEBAF at Higher Energies* edited by N. Isgur and P. Stoler, CEBAF - 1994.
- [34] L L. Frankfurt and M. I. Strikman, *Nucl. Phys.* **A405** 557 (1983).
- [35] T. de Forest, *Nucl. Phys.* **A392** 232 (1983).
- [36] L L. Frankfurt and M. I. Strikman, *Nucl. Phys.* **B250** 143 (1985).
- [37] G. Kälbermann, L. L. Frankfurt and J. M. Eisenberg, *Phys.Lett*, **B329** 164 (1994).
- [38] H. Arenhövel, in *Modern Topics in Electron Scattering*, Edited by B. Frois and I. Sick, 1991, p.136.
- [39] E. D. Bloom and F. Gilman *Phys. Rev.* **D4** 2901 (1971).
- [40] P. Stoler *Phys.Rep.* **226** 103 (1993).
- [41] G. F. Bertsch L. L. Frankfurt and M. I. Strikman *Science* **259** 773 (1993).
- [42] G. E. Brown, M. Buballa, Zi Bang Li and J. Wambach SUNY-NTG-94-54, October 1994.
- [43] P. F. Shepard, T. J. Devlin, R. E. Mischke, J. Solomon, *Phys. Rev.* **D10** 2735 (1974).
- [44] I. P. Auer, *et al*, *Phys. Rev. Lett.* **46** 1177 (1981).

Figure Captions

Figure 1. Graphs for $d(e,e'p)n$ scattering. (a) - Born (PWIA) approximation; (b) - final state interaction contribution, where the broken line accounts for all NN multiple scatterings; (c) - meson exchange current contribution.

Figure 2. The dependence of transparency - T (eq.(49)) on the spectator neutron angles, for different values of neutron momenta: (a) $p_n = 100 \text{ MeV}/c$, (b) $p_n = 200 \text{ MeV}/c$, (c) $p_n = 300 \text{ MeV}/c$ and (d) $p_n = 400 \text{ MeV}/c$. The solid-straight line is the Born approximation, dashed line - contribution of interference between Born and FSI amplitude, dash-dotted - effects of screening - is the sum of Born and interference terms, dotted line - contribution of the double scattering term, solid-line - is the sum of all terms in the cross section. $Q^2 = 6 \text{ (GeV}/c)^2$.

Figure 3. Q^2 dependence of transparency T defined according to eq.(49) at $x = 1$. Solid line - GA prediction, dashed line - CT prediction within QDM approximation, with $\Delta M^2 = 0.7 \text{ GeV}^2$ and dotted line PWIA prediction. Curves labelled "I" are the calculations at $p_n = 0$, "II" - at $p_n = 100 \text{ MeV}/c$, "III" - at $p_n = 200 \text{ MeV}/c$ "IV" - at $p_n = 300 \text{ MeV}/c$, and "V" - at $p_n = 400 \text{ MeV}/c$.

Figure 4. Q^2 dependence of transparency T defined according to eq.(49) normalized on GA calculations: dash-dotted line GA approximation, dotted line - QDM prediction at $p_n = 200 \text{ MeV}/c$, solid line - QDM prediction at $p_n = 300 \text{ MeV}/c$ and dashed line - QDM prediction at $p_n = 400 \text{ MeV}/c$. The curves labelled by boxes correspond to Q^2 dependence of QDM predictions for $R(Q^2, p_{n1}, p_{n2})$ defined according to eq.(51), normalized on GA calculations. Solid line with "boxes" - $p_{n1} = 300 \text{ MeV}/c$, $p_{n2} = 200 \text{ MeV}/c$ and dashed line with "boxes" - $p_{n1} = 400 \text{ MeV}/c$, $p_{n2} = 200 \text{ MeV}/c$. QDM predictions calculated with $\Delta M^2 = 0.7 \text{ GeV}^2$. $x = 1$.

Figure 5. Q^2 dependence of transparency T at $p_n = 200 \text{ MeV}/c$ - (a) and $p_n = 300 \text{ MeV}/c$ - (b), for $x = 1$. The solid-line - prediction within the GA, dotted line - QDM

approximation with $\Delta M^2 = 0.7 \text{ GeV}^2$, dashed line three resonance model within modified GA, with parameters $M_{N^*} = 1.4 \text{ GeV}$, $M_{N^{**}} = 1.8 \text{ GeV}$, $\epsilon = 0.17$, $\frac{F_{N,N}}{F_{N,N^{**}}} = 1.0$ and $\frac{F_{N^*,N}}{F_{N,N^{**}}} = 3.1$. Solid and dashed lines labelled by boxes are calculations within the GA and three resonance model of CT within Green function method and zero-range NN scattering approximation. The parameters for three resonance model are same as above.

Figure 6. Transverse momentum dependence of unpolarized density matrices - $\rho_d(k, k) = u(k)^2 + w(k)^2$ (eq.(16)) - dashed line and polarized density matrices - $\rho_{20}^d(k, k)$ (eq.(53)) - solid line, at $p_n^z = 0$.

Figure 7. The (θ_n, p_n) dependence of asymmetry defined by Eq.(54). (a) - Born (PWIA) approximation, (b) - Glauber approximation. $Q^2 = 6 \text{ (GeV/c)}^2$.

Figure 8. Q^2 dependence of asymmetry defined according to eq.(54), at $x = 1$. Solid line - Glauber approximation, dashed line - QDM of color transparency, dash-dotted line - the three resonance model of color transparency within the modified GA. Straight-dotted line - Born approximation. (a) - $p_n = 250 \text{ MeV/c}$, (b) - $p_n = 300 \text{ MeV/c}$, (c) - $p_n = 350 \text{ MeV/c}$ and (d) - $p_n = 400 \text{ MeV/c}$. QDM and three resonance model parameters are same as in Fig.5.

Figure 9. Q^2 dependence the ratio $R(Q^2, p_{n1}, p_{n2})$ defined according to eq.(51), at $p_{n1} = 300 \text{ MeV/c}$ and $p_{n2} = 200 \text{ MeV/c}$ - (a) and asymmetry A_d defined according to eq.(54) at $p_n = 300 \text{ MeV/c}$ - (b). $x = 1$. Solid line - Glauber approximation, dashed line - QDM approximation with $\Delta M^2 = 0.7 \text{ GeV}^2$, dotted line - $\Delta M^2 = 0.9 \text{ GeV}^2$ and dash-dotted line - $\Delta M^2 = 1.1 \text{ GeV}^2$

Figure 10. The theoretical uncertainties in determining of Q^2 dependence of transparency $R(Q^2, p_{n1} = 300, p_{n2} = 200)$ - (a) and asymmetry $A_d(p_n = 300)$, at $x = 1$. Solid-line - glauber approximations, dashed - lines QDM approximations. Upper, down solid, dashed lines at $Q^2 = 1 \text{ (GeV/c)}^2$ - are the GA and QDM predictions

with Paris and Bonn wave functions respectively. The curves inside corresponds to predictions with Paris light cone wave function, color screening effects (which according to eq.(56) appears at $Q^2 > 2 (GeV/c)^2$) and predictions with different approximation for σ_{en} (eq.(12)). QDM calculated with $\Delta M^2 = 0.7 GeV^2$.

Figure 11. Q^2 dependence the ratio $R(Q^2, p_{n1}, p_{n2})$ defined according to eq.(51), at $p_{n1} = 300 MeV/c$ and $p_{n2} = 200 MeV/c$ - (a) and asymmetry A_d defined according to eq.(54) at $p_n = 300 MeV/c$ - (b). $x = 1$. Solid line - Glauber approximation, dashed line - three resonance model of CT, within modified Glauber approximation, dotted line - QDM approximation of CT, solid line with "boxes" - Glauber approximation with β factor considered in eq.(62) and dashed line with "boxes" - three resonance model of CT, within modified Glauber approximation and with β factor corresponding to higher mass excitation in the intermediate state. QDM and three resonance model parameters are same as in Fig.5.

Figure 12. The θ_n dependence of ratio R . Curve marked by "GA" shows the ratio of $d(e, e'p)n$ cross section calculated within Glauber approximation, without factor of β (eq.(63)) to the PWIA cross section, "GA'" - same as above, with Glauber cross section calculated with factor β , "NM" - ratio of cross section with multiple scattering and Siegert operator to the Born cross section, which also accounts for the direct productions of slow neutrons, "NM+MEC" - "NM" calculation with meson exchange currents, and "NM+MEC+IC" - "NM" calculation with meson exchange currents and isobar contribution. The last three curves are those of the calculation of Ref.[10] for $p_n = 400 MeV/c$ and $Q^2 = 1 (GeV/c)^2$.

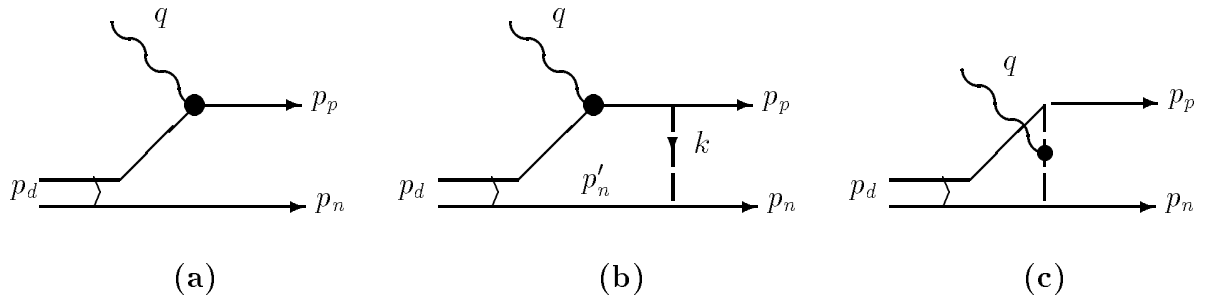


Fig. 1

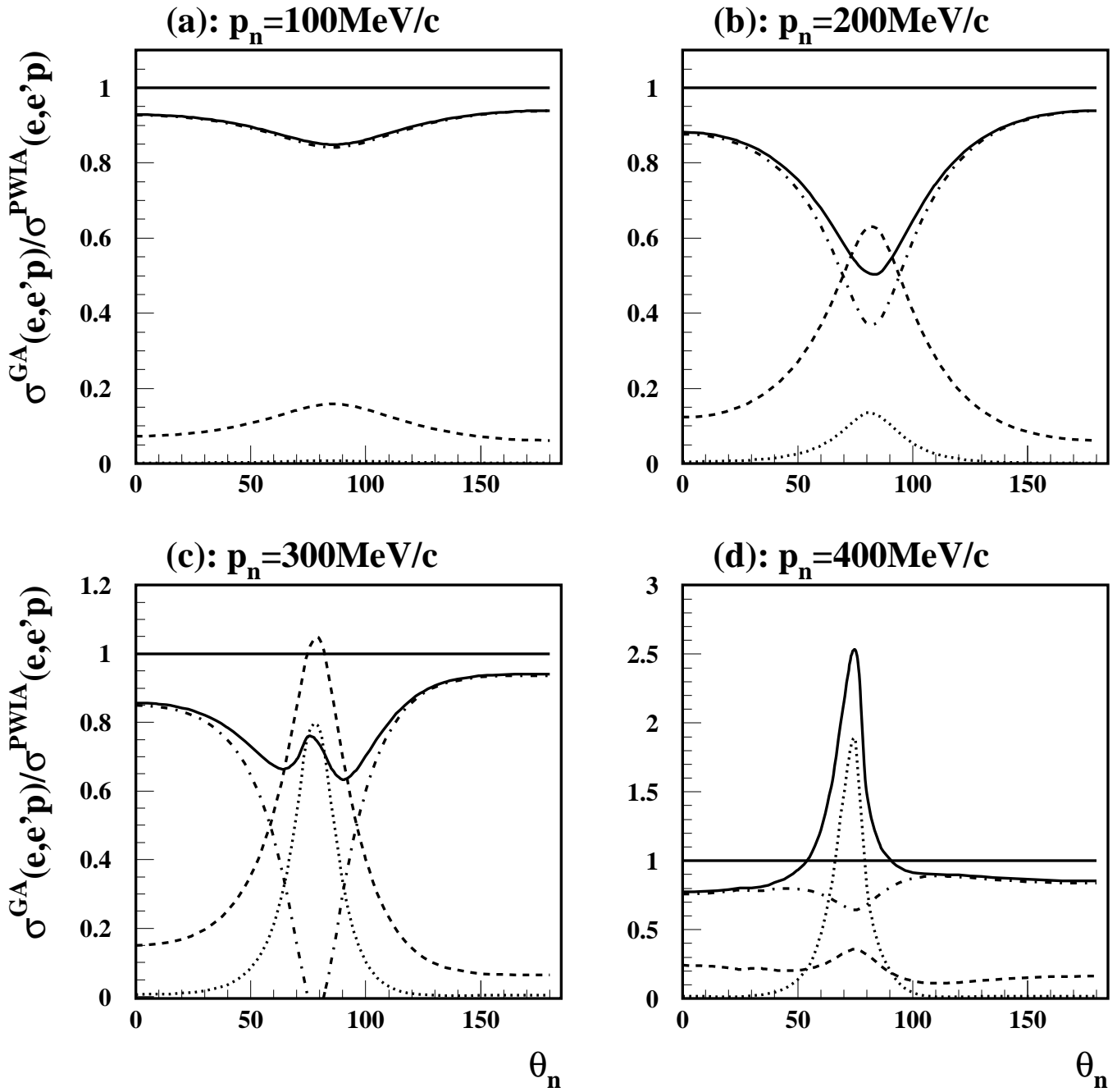


Fig.2

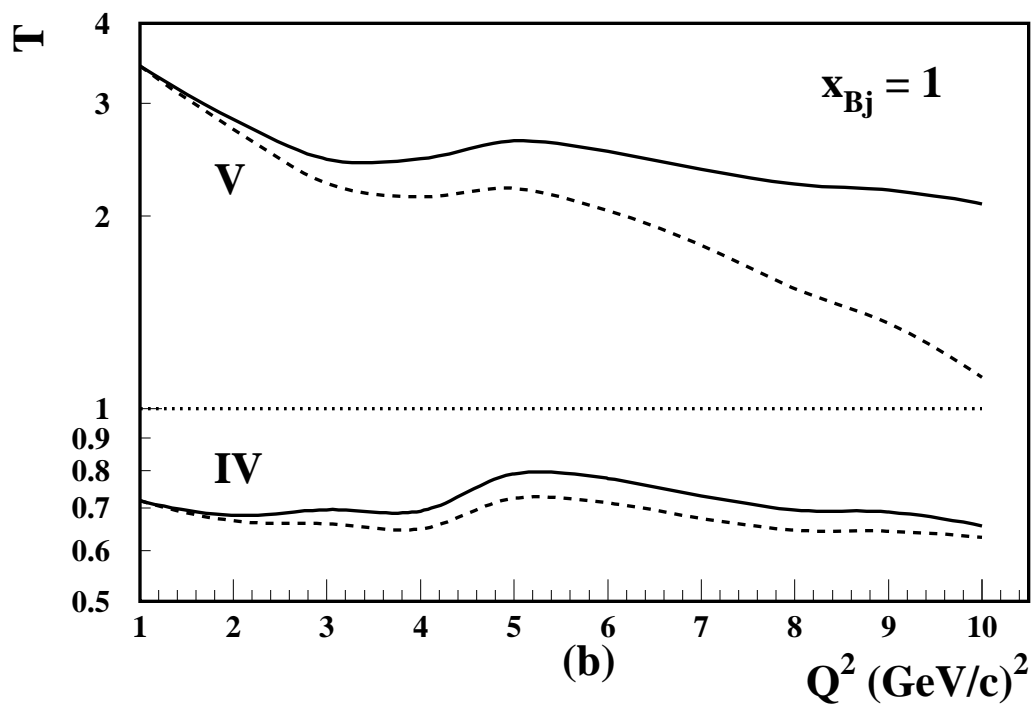
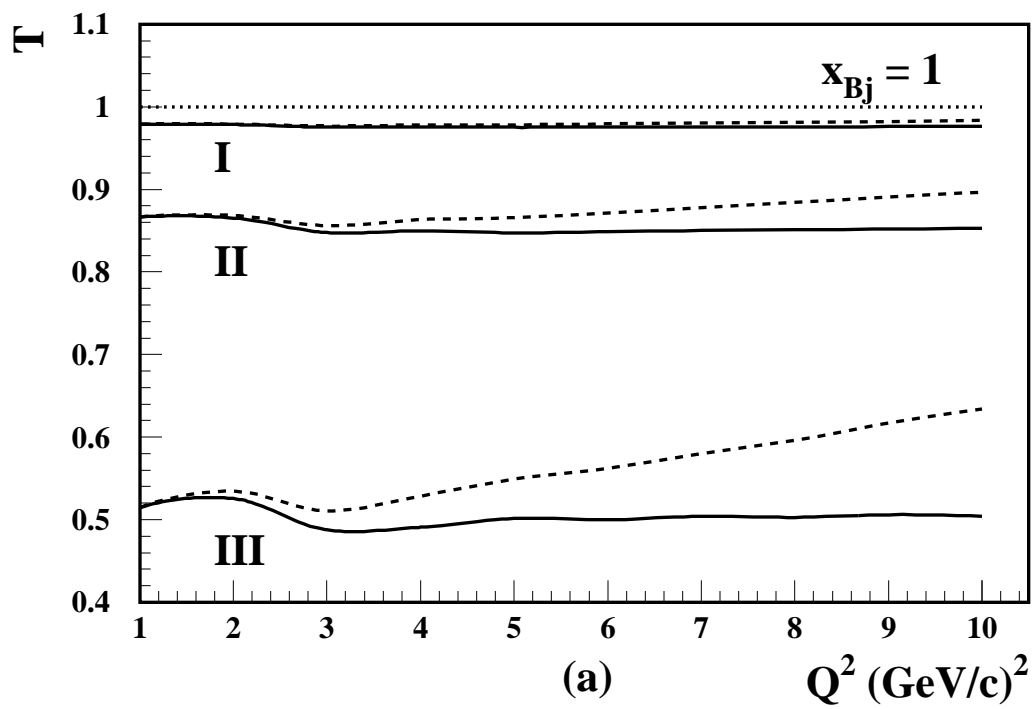


Fig.3

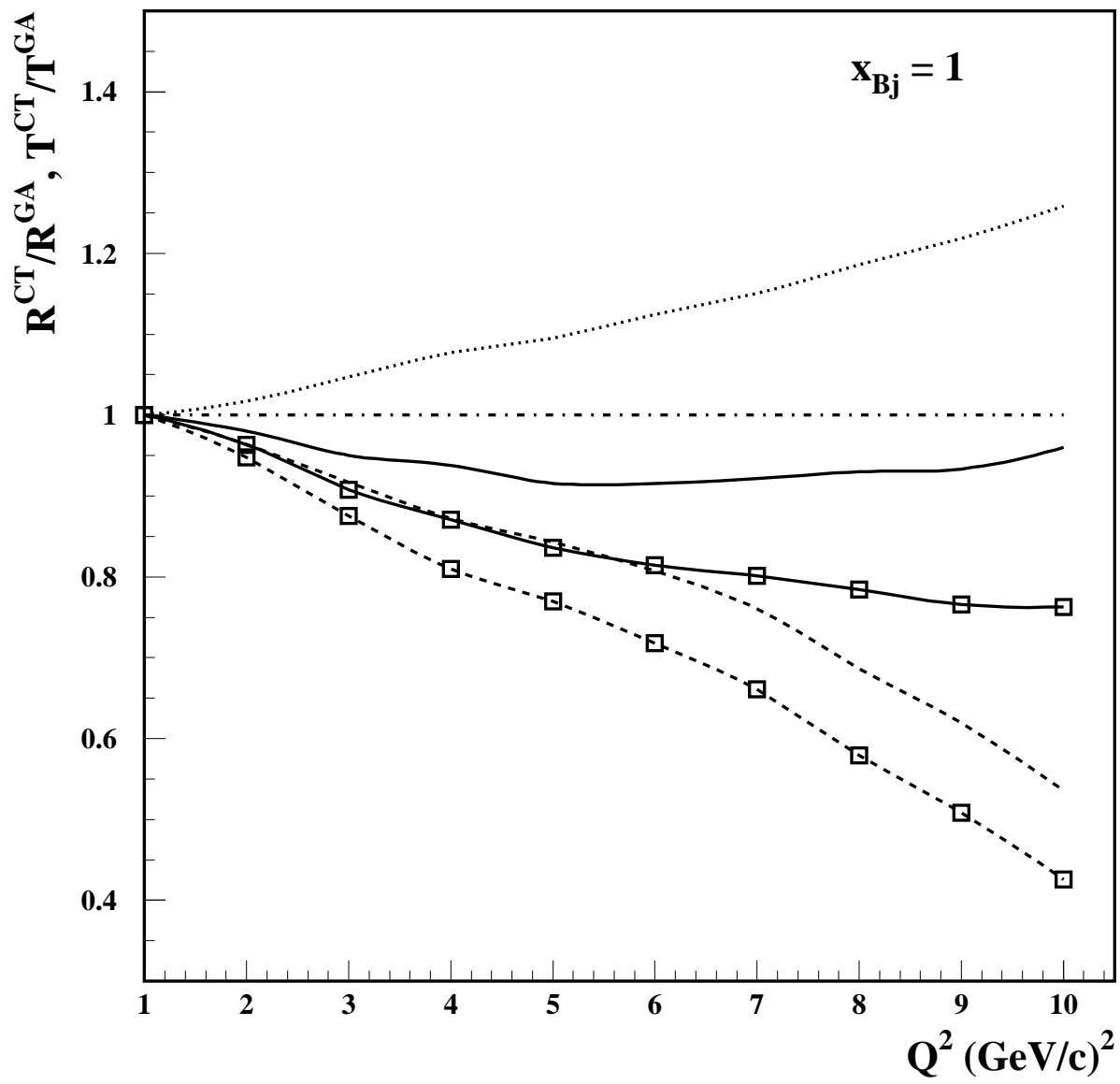


Fig.4

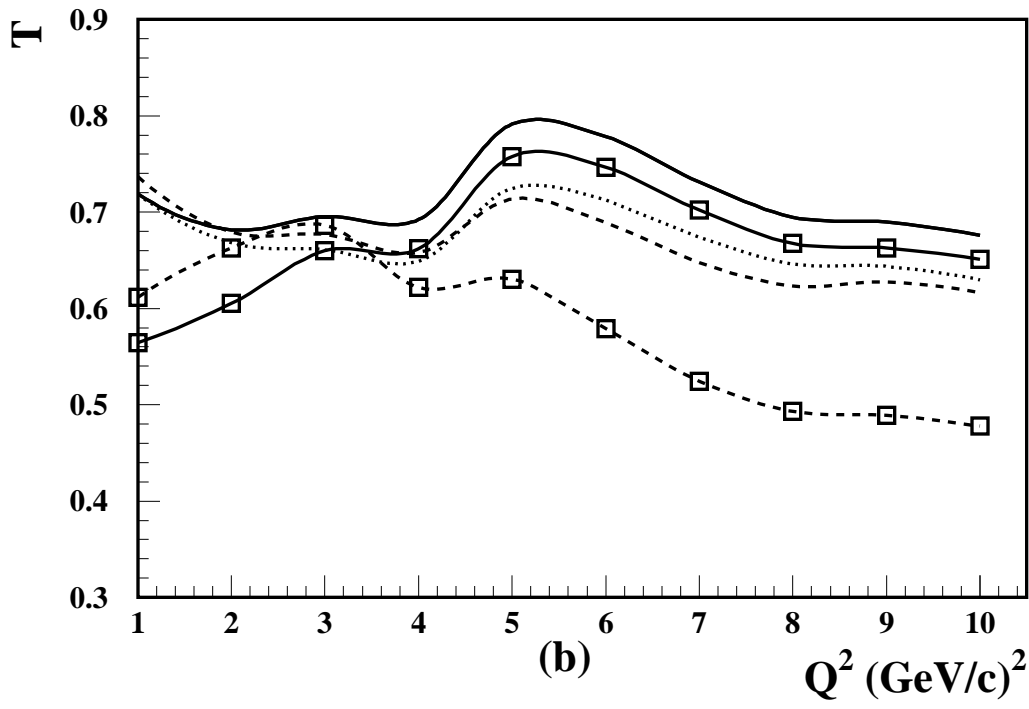
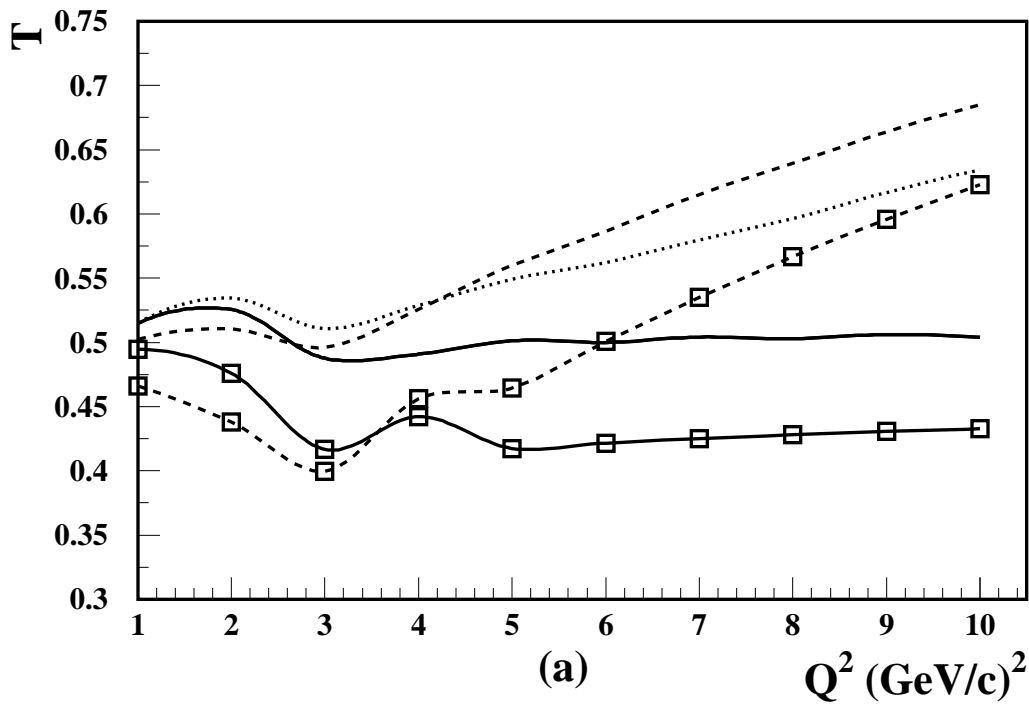


Fig.5

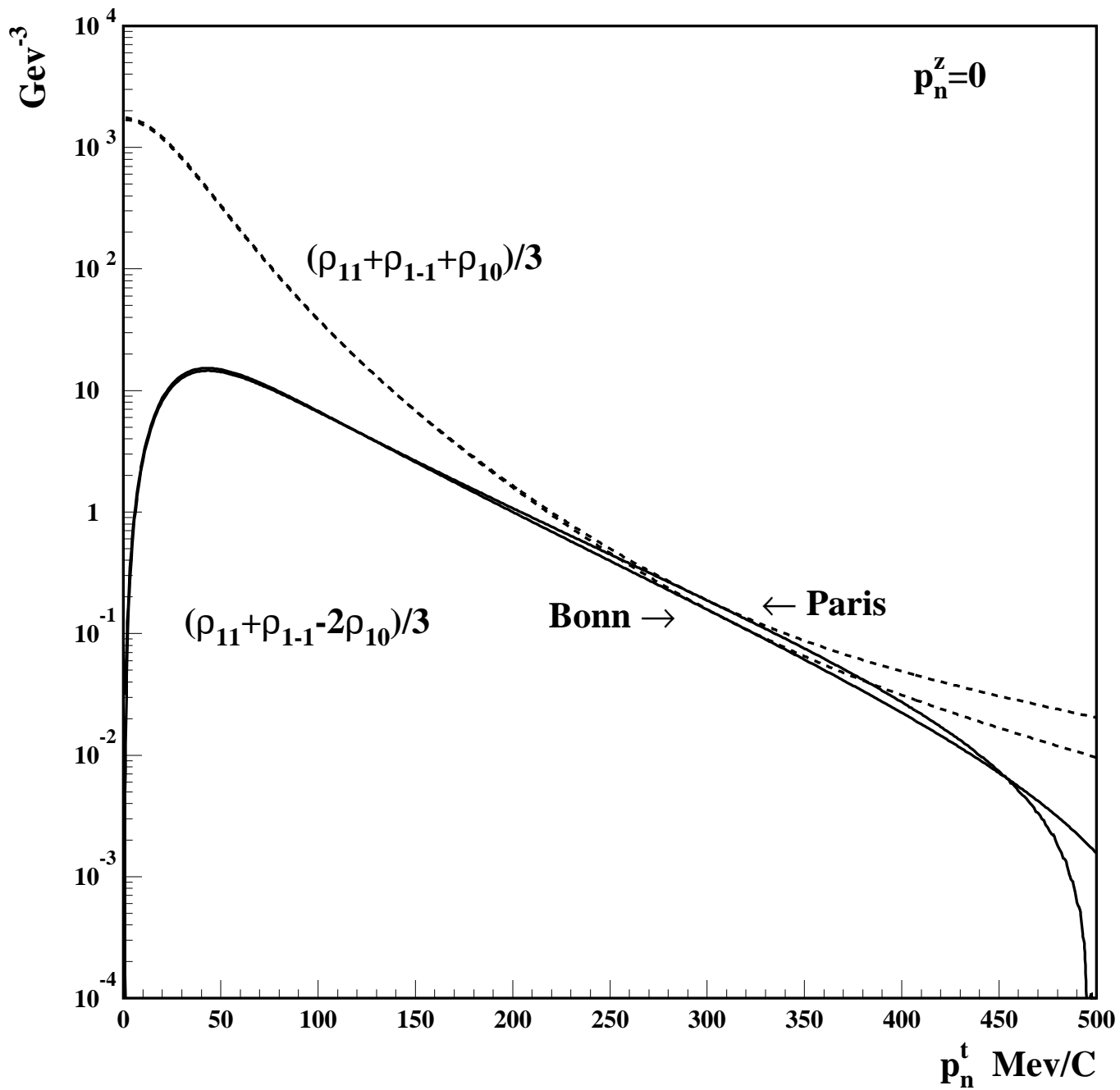
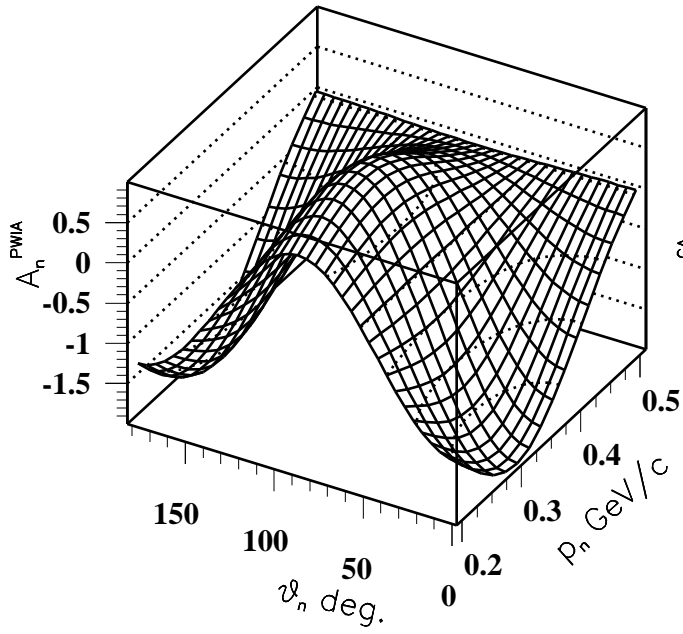
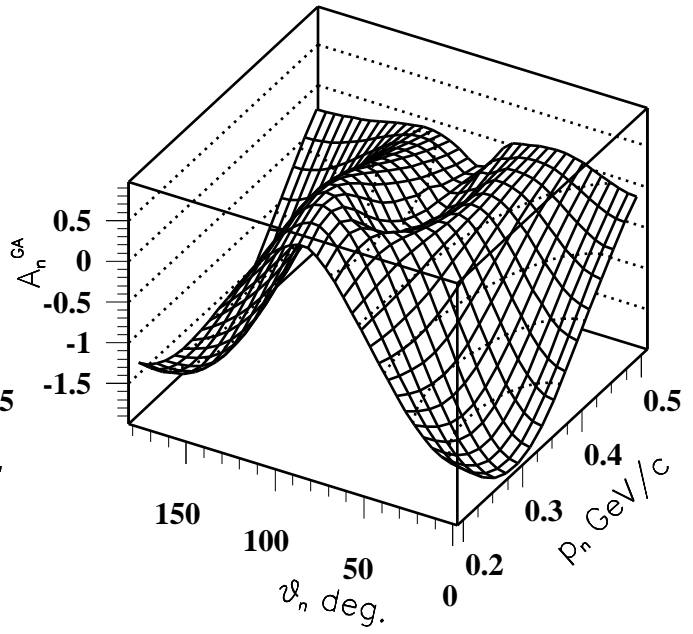


Fig.6



(a)



(b)

Fig.7

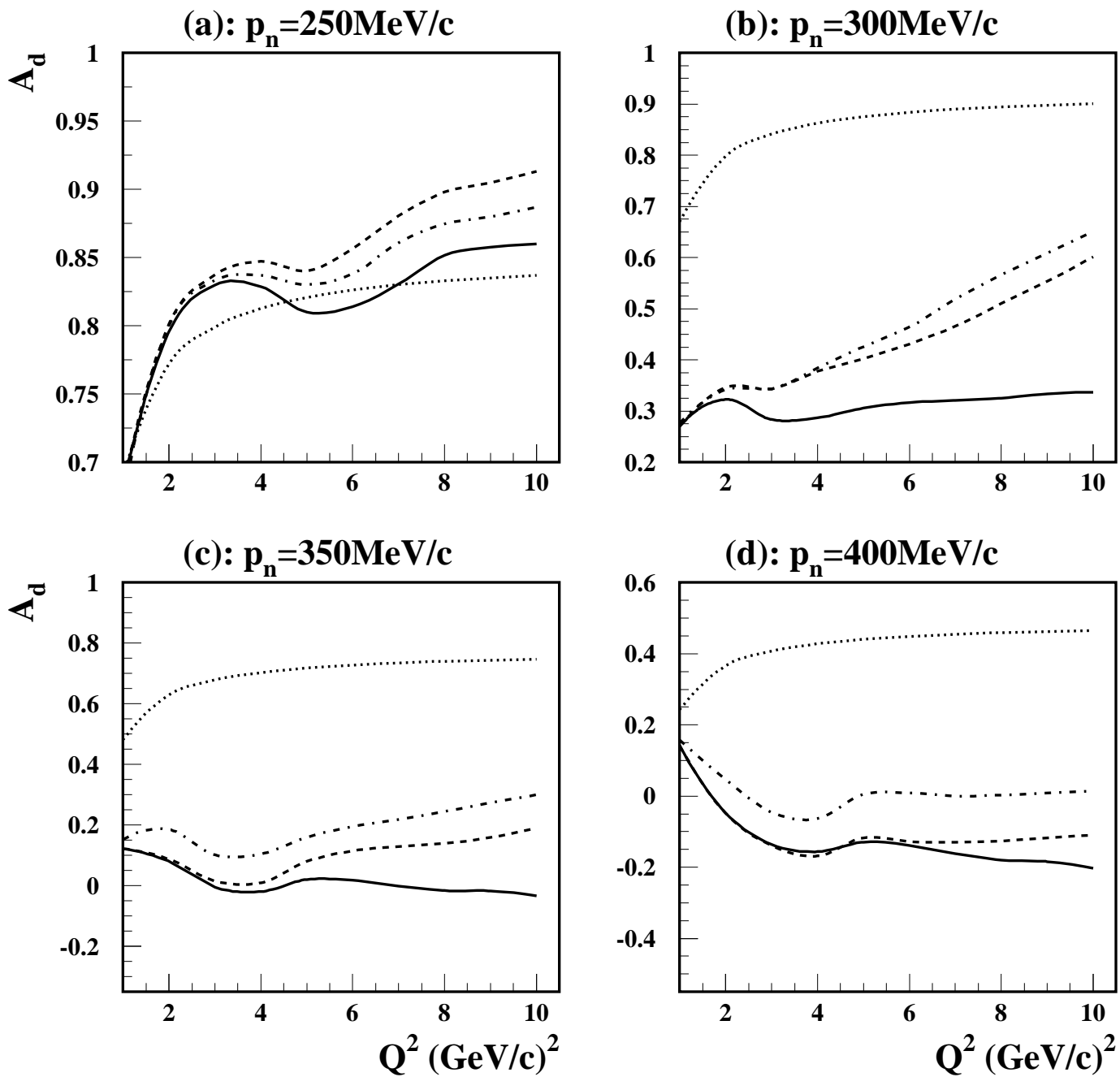


Fig.8

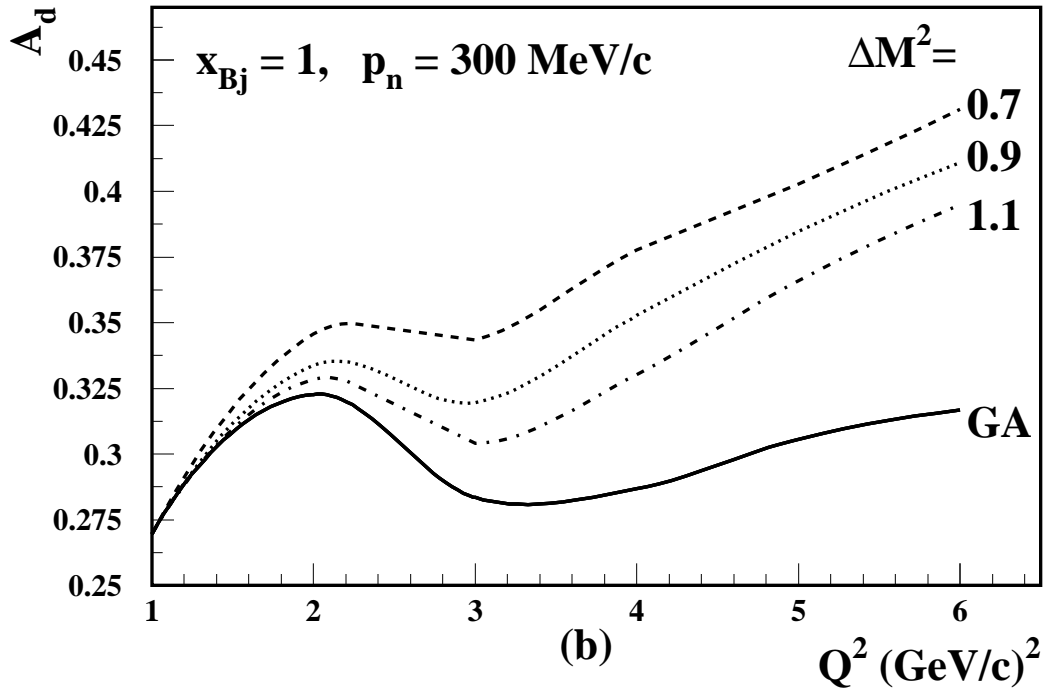
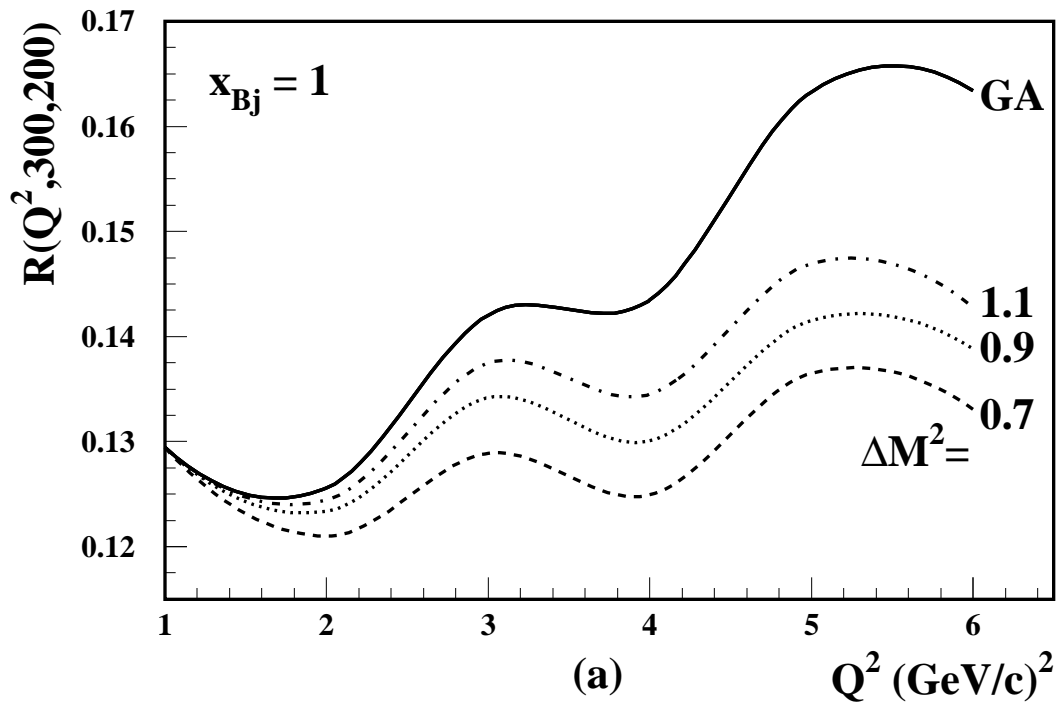


Fig.9

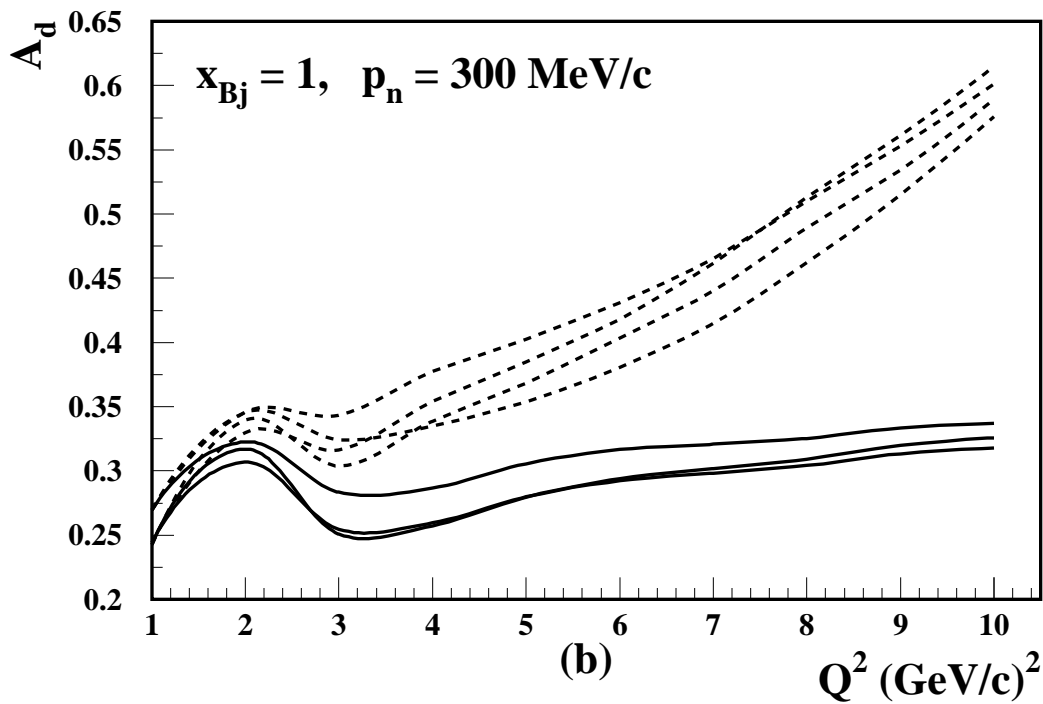
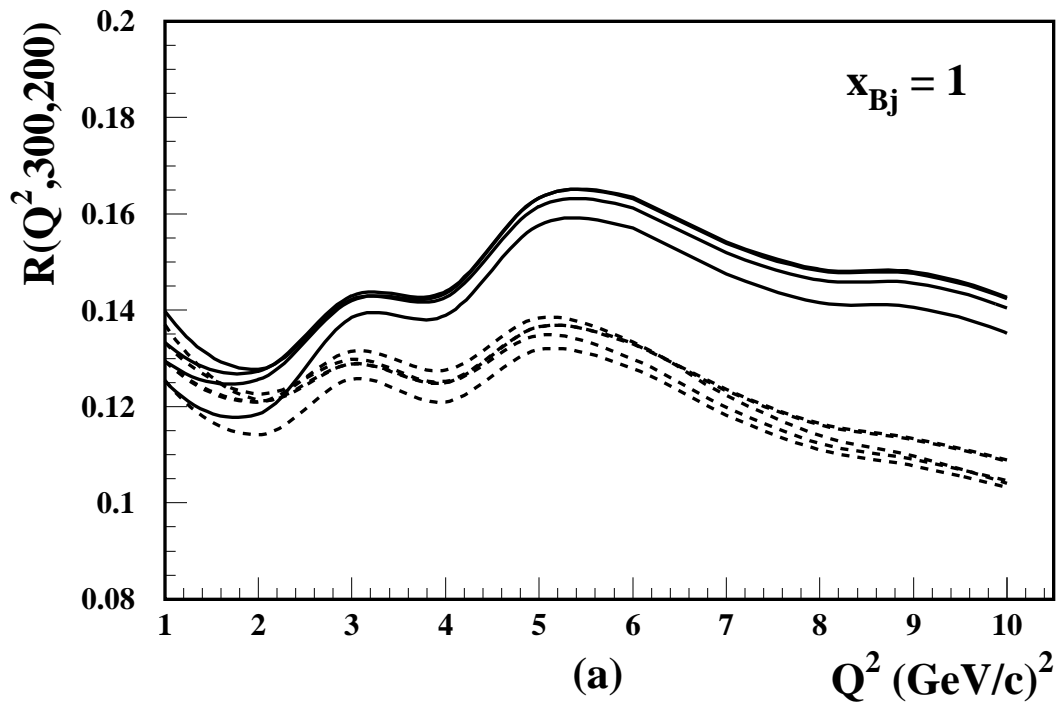


Fig.10

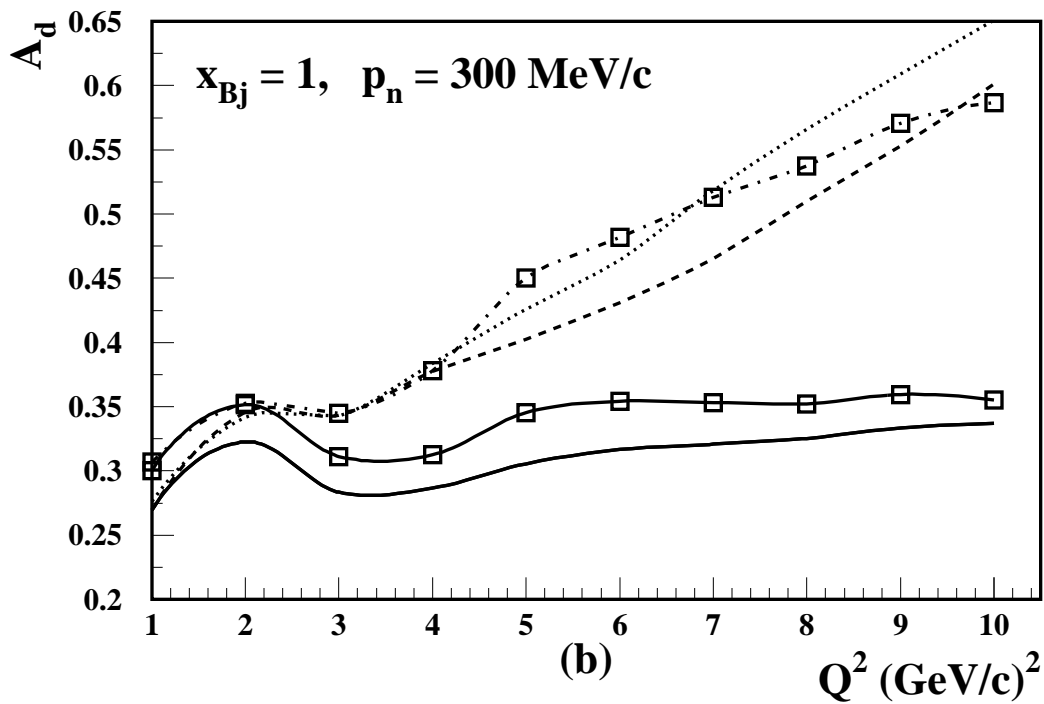
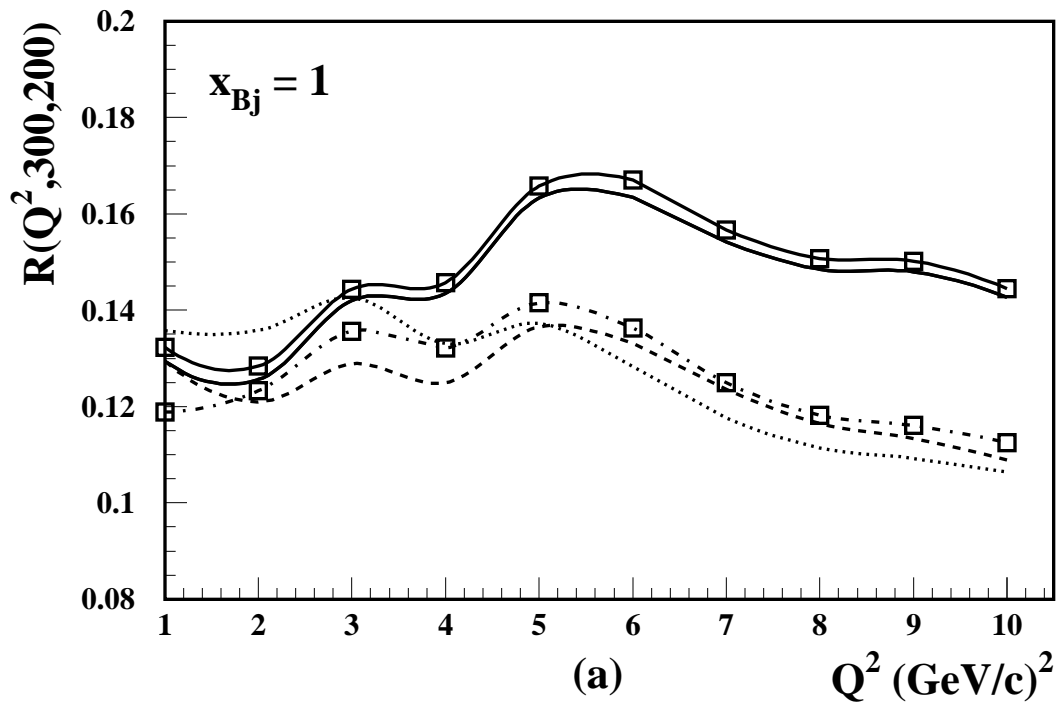


Fig.11

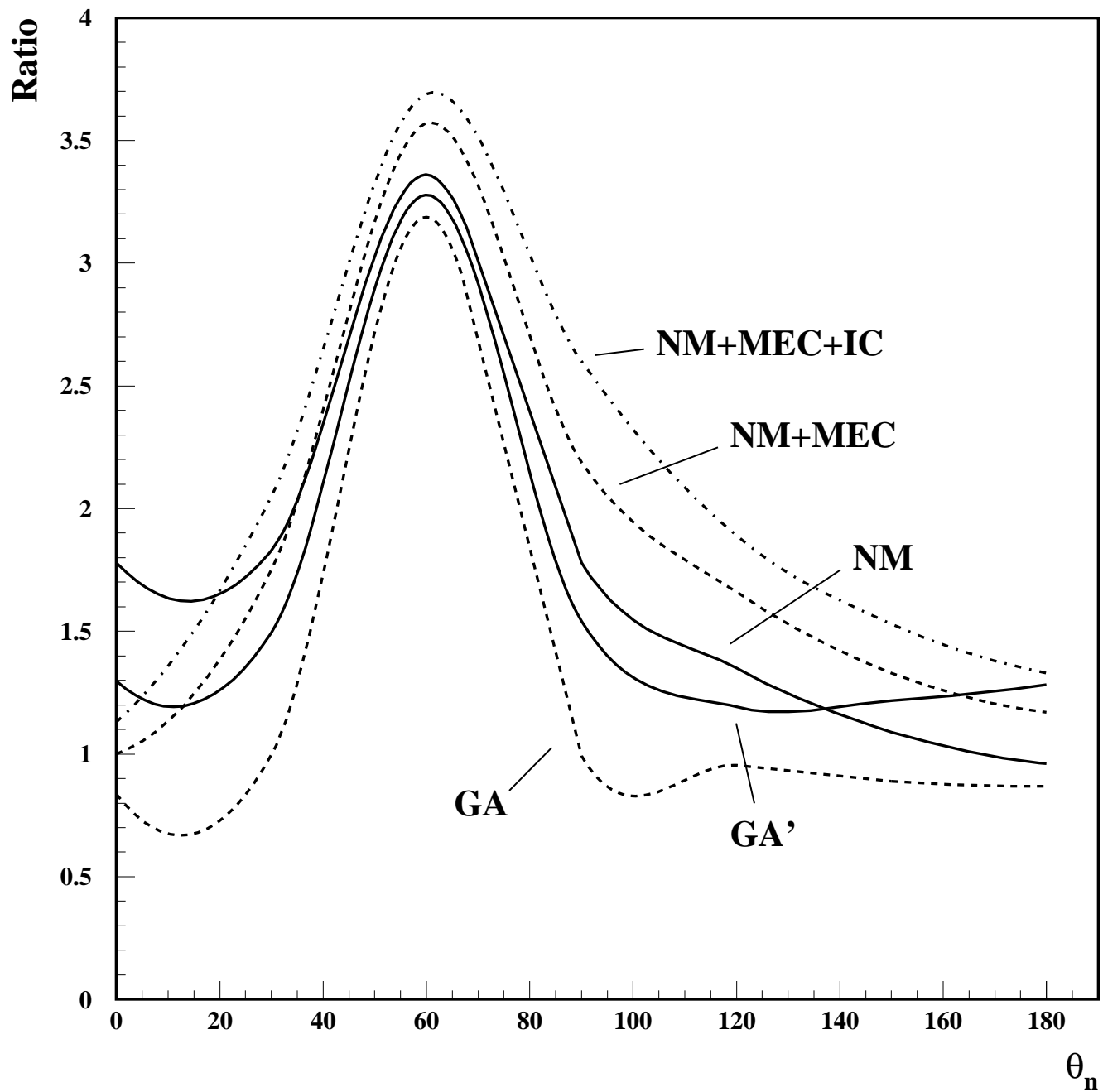


Fig.12